Title

STUDIES OF OPTICAL PULSATIONS FROM HZ Her-Her X-l: A DETERMINATION OF THE MASS OF THE NEUTRON STAR

Author

Middleditch, John.

Publication Date

1975-07-01

Submitted to the Astrophysical Journal

LBL-4282
Preprint c.1

STUDIES OF OPTICAL PULSATIONS FROM HZ Her-Her X-1: A DETERMINATION OF THE MASS OF THE NEUTRON STAR

John Middleditch and Jerry Nelson

July 1975

Prepared for the U. S. Energy Research and Development Administration under Contract W-7405-ENG-48

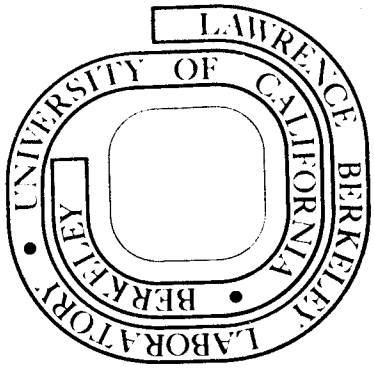

DISCLAIMER

LBL-4282

STUDIES OF OPTICAL PULSATIONS FROM HZ Her-Her X-1: A DETERMINATION OF THE MASS OF THE NEUTRON STAR

John Middleditch and Jerry Nelson

Lawrence Berkeley Laboratory
University of California
Berkeley, California 94720

ABSTRACT

In 500 hours of optical observations of this binary system we have repeatedly detected optical pulsations at the 0.1 - 0.3% level. These pulsations are present only for particular well-defined values of the binary and 35-day phases. Positions of the pulsation-emitting regions, projected onto the orbital plane, have been measured and three distinct regions have been resolved. A simple model is put forth which accounts for the observed binary behavior, which gives a direct determination of the mass ratio, $M_{HZHer}/M_{HerX-1} = 1.68 \pm 0.10$ and which establishes that the spin of the pulsar is prograde. Additionally, it is shown that Hz Her fills its Roche lobe. Using the above, the known X-ray eclipse duration, and the mass function, we calculate the orbital inclination to be $i = 87^\circ \pm 3^\circ$ and the masses to be $M_{HerX-1} = 1.30 \pm 0.14\ M_\odot$ and $M_{HZHer} = 2.18 \pm 0.11\ M_\odot$.

I. INTRODUCTION

The dramatic discovery of the eclipsing binary system containing the X-ray source Hercules X-1 by Tananbaum et al (1972) was rapidly followed by the identification of an optical counterpart, HZ Herculis (Bahcall and Bahcall 1972; Forman, Jones and Liller 1972; Davidsen et al 1972). The first substantial observations of optical pulsations were reported by Davidsen et al (1972; hereafter Paper I). These, and additional observations were described in some detail by Middleditch and Nelson (1973; hereafter Paper II). Groth (1974) has also reported the detection of optical pulsations. A number of negative searches for pulsations have been reported (Groth and Nelson 1972; Frolich 1973; Cocke et al 1973) but in each case the lack of success is attributable to a lack of sensitivity or to observing at an inappropriate binary phase. Paper II discusses this problem, and the present paper will indicate in detail the complex time behavior of the pulsations.

It is generally agreed that most of the light coming from the system results from the heating of the surface of HZ Her by X-rays from Her X-1. If, as seems likely, the X-ray flux is strongly modulated at the 1.24 s period, it is interesting to ask what degree of modulation one would expect in the optical light. Basko and Sunyaev (1973), Dahab (1974), and Alme and Wilson (1974) have estimated a timescale of seconds for the emission in the visible continuum from the heating of the surface of HZ Her. On the other hand, Davidsen, Margon and Middleditch (1975; hereafter Paper III) have reported detections of optical pulsations (within runs 116 and 125 of this paper) from HZ Her associated with the rapidly (< 0.1s) re-emitting emission lines of He II and N III. The details of such processes are essential to understand the strength of optical pulsations actually seen.

As we will discuss, the behavior of the optical pulsations is sufficiently dictated by the geometry of the binary system that many basic parameters of the system can be found without a detailed understanding of the emission mechanisms.

We will argue that the nature of the optical pulsation data defines the geometry of the system; the Roche lobe is essentially filled and the mass ratio $M_{HZHer}/M_{HerX-1} = 1.68 \pm 0.10$. The same arguments show that the pulsar rotation is prograde. Combining these results with the known x-ray eclipse duration will yield the actual masses of both components, $M_{HZHer} = 2.18 \pm 0.11\ M_{\odot}$ and $M_{HerX-1} = 1.30 \pm 0.14\ M_{\odot}$.

Our observations indicate not only optical pulsations from the surface of HZ Her, but also from a region near Her X-1. These pulsations give clues about the characteristics of the accreting disk and the accreting stream.

The interpretation of data from the HZ Her-Her X-1 system is made particularly difficult by the presence of the 35-day cycle seen in the X-ray data, in the slow photometric data (Deeter et al 1975), and in our own pulsation data. Our understanding of this cycle is incomplete at best, so the final test of many ideas on the behavior of the system must await a reasonable understanding of this phenomenon.

In § II we briefly describe the data acquisition, the analysis procedures, and the sensitivities of the Fourier transform and signal averaging techniques used. In the data presentation (§ III) we describe the nature of the optical pulsations as inferred by means of these analysis procedures. These procedures make no strong assumptions on the physical processes involved in HZ Her-Her X-1. In § IV we describe the possible implications of the observations and develop a model of the binary system

which describes much of the observed behavior of the system. We summarize the salient features in the reduced data and describe the assumptions, successes and failures of the model calculation in the concluding section.

II. DATA COLLECTION AND REDUCTION PROCEDURES

During the period July 1972 through September 1974, we observed HZ Her on 120 nights, collecting about 540 hours of data. The data were taken with an unfiltered, dry-ice cooled EMI-9658R photomultiplier tube with an S20 photocathode. The phototube assembly was mounted on the Lick Observatory 61 cm Cassegrain reflector.

The numbers of detected photons in successive 40 ms time intervals were recorded digitally on magnetic tape for each run. These numbers were prescaled by division and subtraction to fit into a six bit word. The apparatus is discussed briefly in Papers I and II and in more detail by Middleditch (1975). The typical count rate from the star alone was between 1000 and 4000 counts/sec, depending on the binary phase. The typical run was about three hours in duration (2^{18} data bins). Photometric calibration before and after each run was made using a blue comparison star with $m_V \simeq 12.7$ (star B of Grandi et al 1974).

The data tapes were analyzed using the Cooley-Tukey fast Fourier transform algorithm and power spectra were obtained by summing the squares of the real and imaginary parts of the complex elements. The analysis to determine the statistical significance of a signal estimated the background noise with a running local average of the power spectrum as described in Paper II and by Middleditch (1975).

Since noise dominates the data sample, the locally defined power P has an exponential probability distribution

$$\text{Prob}(P)\, dP = e^{-P}\, dP \qquad (1)$$

thus the probability that any given power level is due to noise rather than an actual signal can readily be calculated. For example, the probability of noise producing a power level ≥ 10 in a given bin is $\sim 5 \times 10^{-5}$. The amplitude of a signal (amplitude of pulsation) was obtained from the following analysis. We define q as the mean squared deviation of the input data in counts^2 s^{-1}, T as the run time in seconds, and r_f as the ratio of average power close to the frequency of interest to the average power for the entire spectrum (excluding $f = 0$). Typically $r_f \simeq 1$. The best value for the signal amplitude, a, necessary to produce an excess power, P_e, in n adjacent power spectrum bins is given by

$$a = \sqrt{4q\, r_f (P_e \pm \sqrt{2P_e + n})/T} \text{ counts s}^{-1} \qquad (2)$$

The quantity, P_e, is given by the formula

$$P_e \sum_{i=1}^{n} (P_i - 1) \qquad (3)$$

where P_i is the power in the i*th* bin of the sequence. When equation (2) is used to evaluate a negative excess power, the minus sign is moved outside of the square root. In this way, negative amplitudes are used to indicate a deficiency of power.

The pulsed fraction for any given run was defined as the ratio of the pulsed amplitude to the fixed light level of a star with $m_v = 13.0$, approximately equal to the maximum HZ Her light level.

Since the best frequency resolution is obtained with longest runs, we usually used data blocks at least 3 hours long to determine accurate pulsation frequencies. The data was also analyzed in shorter blocks (at

most 3 hours) to study the temporal behavior of the pulsation amplitude and determine pulsed fractions.

The period (1.700165 days) and epoch (JD 2,441,506.3921 UT) used to determine the orbital phase were taken from the X-ray observations of Giacconi et al (1973). The 35-day phase was calculated in cycles from a set of epoch fiducials fixed in the midpoint of the hard X-ray "off" interval. When X-ray "turn-ons" were observed near orbital phases 0.23 or 0.68 (0.00 = eclipse), the fiducial of the current 35-day epoch was fixed to precede the "turn-ons" by 7.23 or 6.68 cycles respectively. Other epoch fiducials which did not have observed turn-ons were established mostly by extrapolation from previous fiducials with an alternating 20 or 21 cycle interval.

The fiducials for the 35-day epochs are given in Table 1. Also given are the dates of the nominal "turn-ons" and the associated 35-day phase. In addition, the number of cycles between the fiducials is listed in the last column. The nominal period of hard X-ray activity extends from near cycle 7.00 to near cycle 14.00. The intervals of the hard X-ray "off" extend from 0.00 to roughly 7.00 and from 14.00 to 20.00 or 21.00. The "turn-on" epochs of Table 1 are consistent with the X-ray observations of Giacconi et al (1973), Davison and Fabian (1974), and McClintock et al (1974).

Table 2 lists our observations, giving the run number, UT calendar date, time of the run center, the 35-day and 1.7-day phases of the run center and the run durations.

The frequency for Her X-1 used in the data analysis was taken to be 0.8078735 Hz or a pulse period of 1.2378175 seconds. This is the average for the period of December 1971 through March 1973 as given by

Giacconi (1975).

A frequency region centered on the average Her X-1 frequency whose width was arbitrarily set to twice the total Her X-1 doppler variation was used to scan the data for significant events (excess power at a single frequency). The cutoff level was set at 10.0 times the average noise level so that only 0.16 accidental events were expected for the entire ensemble of power spectra used for good frequency resolution.

Significant events were detected on 28 different nights. The frequencies of pulsation for these signals were measured more accurately than the nominal $\pm$ 1/2T resolution ($\delta f \sim 5 \times 10^{-5}$ Hz for T = 3 hours) of the power spectra with a signal averaging procedure described by Middleditch (1975). The resolution achieved by this procedure is

$$\delta f = 3/(\pi T \sqrt{6P}) \text{Hz} \qquad (4)$$

where T is the run time in seconds, and P is the power associated with the pulsation.

The time derivative of the frequency for a given run can also be found by appropriate signal averaging procedures (Middleditch 1975). This is determined with a precision

$$\delta f' = \frac{\sqrt{90}}{\pi T^2 \sqrt{P}} \text{ Hz/s} \qquad (5)$$

Table 3 lists the frequencies and their time derivatives and the associated errors for the more significant events. The run numbers, calendar dates, durations, and power maxima are also given.

With some assumptions, f and f' can be used to determine the origin of the pulsed light within the binary system. If the detected pulsations come from a corotating region in the binary system and if the excitation

of that region is caused by Her X-1 (the clock in the system), then the spatial coordinates of that region (projected onto the orbital plane) are specified by f and f'.

Briefly, one can see this as follows: Assume the observer is looking into the system edge-on ($i = 90°$), and that the orbit is circular. Define a cartesian coordinate system fixed relative to the observer with its origin at the center of mass of the system, its y axis pointing towards the observer, and its z axis parallel to the system angular velocity, $\vec{\omega}$. Then a small "reflecting" region at (x,y) fixed in the binary system will emit pulsations with a doppler shifted frequency

$$f = f_0 \left(1 + \frac{\omega x}{c}\right) \tag{6}$$

and a rate of change given by

$$f' = \frac{f_0 \omega^2}{c} y$$

where f_0 = Her X-1 frequency = 0.8078735 Hz, and ω = orbital angular velocity = 4.277353×10^{-5} rad/s. Consequently, values of f and f' yield the source position projected into the orbital plane

$$\begin{aligned} x \pm \delta x &= (f - f_0 \pm \delta f) \frac{c}{\omega f_0} \\ y \pm \delta y &= (f' \pm \delta f') \frac{c}{\omega^2 f_0} \end{aligned} \tag{7}$$

It is now straightforward to transform these coordinates to a projected position fixed in the binary system. It is worth noting that with only the nominal Fourier transform frequency resolution of $1/2T$, a 3 hour run still enables one to measure velocities in the binary system with a precision of

$$\delta v = c \frac{\delta f}{f} \sim 18 \text{ km/s} \qquad (8)$$

III. DATA PRESENTATION

While optical pulsations from the Her X-1 system are weak and intermittent, the great sensitivity of Fourier transform techniques allows one to measure these small signals. A great deal of observing time has also enabled us to describe a good deal of the complex time behavior of the system.

A segment of a power spectrum covering the Her X-1 pulsar frequency is shown in Figure 1(a). Frequency is measured along the horizontal scale and for convenience, the relative velocity in the binary system using $v = c(f - f_0)/f_0$ is also indicated. The vertical scale shows the local power level. To show schematically the connection with Her X-1, a circular orbit is exhibited indicating the binary phase interval of the observation (darkened segment). It is scaled to permit the location of the expected Her X-1 pulsar frequency by simply projecting it onto the horizontal axis. In this example the binary phase is ~ 0.25 and an unambiguous signal is seen, clearly at a different frequency than that expected from Her X-1 at this binary phase.

A second power spectrum, exhibiting unusual structure, is shown in Figure 1(b). Significant power was detected at two distinct frequencies, only one consistent with the expected Her X-1 frequency. The occurrence of significant power at more than one frequency in a given run is rare. The great majority of runs with excess power show only a single bin (or adjacent bins) with a notable power level.

To give a qualitative indication of the pulsed power, we have constructed a power spectrum consisting of the sum of all individual spectra. This summary is shown in Figure 1(c). No corrections have been made to compensate for the sampling biases or the differing sensitivities from night to night, thus no quantitative information can be drawn from this figure. Excess power is evident in the frequency interval surrounding the nominal Her X-1 frequency. Some excess is also seen at a frequency near that of Her X-1 at phase 0.75. Note that no excess power is discernible outside the range of frequencies (or velocities) of Her X-1.

To help in understanding the nature of the observed pulsations, a plot of frequency versus binary phase is very useful. On such a plot, a single bin in a power spectrum is represented by a box of fixed area since the frequency resolution is proportional to the run length.

Figure 2(a) shows this plot with only the most significant (Power > 10 exponential levels, noise probability $< 5 \times 10^{-5}$) events plotted. The vertical scale is shown both in frequency and velocity units. For reference, a solid horizontal line at the actual Her X-1 frequency is plotted. A sine wave (solid line) is also plotted showing the expected Her X-1 frequency as a function of binary phase. It is apparent that the bulk of the excess power of these events is located in three regions of this figure. These are labeled I, II and III (the pulsations within each region will be referred to as Features I, II and III). To understand more fully the nature of these regions, data from all runs, not just those with the strongest signals, should be considered. We arbitrarily define a region in phase-frequency (profile B) which covers the expected Her X-1 frequency and has a width of $\pm$ 0.1 Δf_{max}. Δf_{max} is just the maximum expected doppler shift of Her X-1. The set of dotted lines indicates this region. We select

from all the power spectra those bins with any overlap on the defined region. We then calculate the mean pulsed fraction as a function of binary phase using the power in the selected bins according to equation (2) and correcting for the observational coverage over the 1.7 day binary period. Figure 2(d) shows the number of times various intervals of binary phase were observed. (The evident non-uniformity of coverage results from selecting as observing nights those times when pulsations were found to be most likely, i.e., phases around 0.25 and 0.75.) Figure 2(c) shows the mean pulsed fraction for data overlapping profile B. The major signal seen here is clearly associated with Region III. We similarly define a sinusoidal band (profile A) which includes Regions I and II. The mean pulsed fraction in this band, for all our data, is then calculated and is shown in Figure 2(b). Signals in Regions I and II show up clearly. Note the absence of any pulsations in the vicinity of binary phase 0.5. The pulsed fraction seen in any of the data and indicated in these figures is remarkably small, usually less than 0.1%.

Because excess power is not always discernible in a single run, we have made cumulative power spectra for various binary phase intervals. This search for excess power has yielded a weak and puzzling pulsation source in the system. While no single run showed unequivocally the presence of excess power in the binary phase region 0.5 - 0.7, summed power spectra [Fig. 1(d)] indicate such a source with 99.9% certainty. The most curious feature is that its frequency corresponds neither to Her X-1 or to a source on the surface of HZ Her as is indicated by Regions I and II. We have no simple model to explain this feature. Speculations on its possible origin are discussed by Middleditch (1975).

Having observed the general behavior pattern of the pulsed power in frequency and binary phase, we may now study the data in more detail. Using the f and f' determinations described above, we have analyzed the runs in Regions I, II and III and calculated the source positions in the binary system. These are plotted in Figure 3. Since the uncertainty in f and f' depend on the signal strength, we have only used those runs with the greatest pulsed power. The error boxes shown are plotted relative to the fixed points of Her X-1 and the center of mass (CM) of the system. Because of its suggestive nature, the center of HZ Her and its associated Roche Lobe for mass ratio 1.7 are also shown. The arrows on each box indicate the direction towards the observer. The shorter side of each box comes from the f error, the longer side, the f' error.

The structure of the data seen in Figure 3 and Figure 2 suggests that the optical pulsations seen in Regions I and II originate from the surface of HZ Herculis, which is highly excited by the X-ray flux from Her X-1. Region III appears to originate from near the X-ray source itself, certainly quite distinct from the locations of Regions I and II. Note also that while Region I and II form a symmetric pair, Region III has no apparent counterpart near phase 0.25.

A simple check on the reliability of the pulsation measurements and the stability of Her X-1 can be made by displaying the data against time rather than folded modulo the 1.7 day period. Figure 4(a) shows the frequencies and equivalent velocities of the strongest signals (see Table 3). No long term drift is evident, and assuming the Region III pulsations originate very near to Her X-1, the absence of significant residuals for this group checks the constancy of the pulsar frequency rather well, as well as corroborating the error estimates made for the frequency of

detected signals.

Before proceeding with the development of a model to explain the presence of Regions I and II, we will briefly discuss our data in terms of the 35-day cycle. Using the 35-day epochs from Table 2, we have folded the pulsation data for Regions I, II and III to show the mean pulsed fraction as a function of 35-day phase in Figure 5. Cycles 0-7 and 14-21 are X-ray "off" and cycles 7-14 are X-ray "on" intervals. The binary phase-frequency region used is shown in the insets of the figure. While Region III [Figure 5(c)] shows the most obvious correlation with the 35-day cycle, both Regions I and II [Figure 5(a)(b)] also show significant correlations. DC photometry of HZ Her by Deeter et al (1975) when displayed for the binary phase intervals of Regions I and II respectively shows magnitude variations with a strikingly similar 35-day phase dependence (Boynton 1975). As yet we have no model to explain this remarkable similarity. We note that because 35-day structure exists, our normalizations using the data sample over a 1.7 day period, particularly for mean pulsed fraction, are subject to some uncertainty and a quantitative interpretation must be carefully treated.

IV. DISCUSSION

a) Features I and II — Reprocessing/Reflection Models

Since Features I and II have been shown to originate from HZ Her, they can be used to measure its velocity in the binary systen and thus along with the known velocity of Her X-1 (169 km/s) establish the mass ratio. To do this we have developed numerical models to simulate the action of the surface of HZ Her in producing pulsations from the periodic X-ray excitations.

We assume that the surface of HZ Her is a Roche equipotential (in corotation). This will be supported by the data and the models discussed below. Usually we have also assumed that the characteristic time to reprocess X-rays into visible light is a constant over the illuminated surface of HZ Her. This is supported by the results of Paper III which established a pulse phase agreement between the photospheric reprocessing of the He II and/or N III lines (known to occur in less than 100 ms) and the broad band pulsations. The effects of variable reprocessing times have also been tested with simple models.

Our coordinate system and notation are defined in Figure 6. We use a Cartesian coordinate system with its origin at the system center of mass, its x axis passing through the center of Her X-1, and its z axis parallel to the system angular momentum. The equation for the Roche equipotential surfaces is given by

$$\phi/GM_{HZHer} = \frac{-r^2(1 + 1/R)}{2a^3} - \frac{1}{\rho'} - \frac{1}{R\rho} = \text{constant} \quad (9)$$

where r, ρ and ρ' are defined in Figure 6 and R is given by

$$R \equiv M_{HZHer}/M_{HerX-1} .$$

The component separation, a, is related to d (the CM to Her X-1 distance) by the equation

$$a = d(1 + 1/R) .$$

X-Ray observations from Tananbaum et al (1972) give

$$d \sin(i) = 3.95 \pm 0.01 \times 10^{11} \text{ cm}$$

where i is the inclination of the orbital system.

Having defined the surface of HZ Her (by specifying ϕ and R) we may now proceed to the model calculation. The apparent optical flux as a function of time is obtained by integrating over the surface of HZ Her. The local, time-dependent surface brightness is a result of the X-ray flux impinging upon it.

Explicitly, the optical flux is given by

$$I(t) = \int_S ds\ V(\hat{o},\hat{\rho})\ L\ (t,\hat{\rho})/4\pi\rho^2 \qquad (10)$$

where

ds is the surface element at (x,y,z)

V is the visibility function at ds

$\hat{o}$ is a unit vector toward the observer

$\vec{\rho}$ is a vector from Her X-1 to the HZ Her surface element ds

and L is the apparent surface brightness at ds .

We define

$$\cos\theta = \hat{o} \cdot \hat{n}$$

$$\cos\psi = -\hat{\rho} \cdot \hat{n}$$

where $\hat{n}$ is the normal at ds. Then we can write

$$V(\hat{o},\hat{\rho}) = V(\cos\theta,\cos\psi) = \cos\theta\ \cos\psi \quad \text{for model 1}$$

$$= \cos\psi \quad \text{for model 2}$$

$$= \cos\theta \quad \text{for model 3}$$

and V = 0 if the surface cannot be seen from the Earth or from Her X-1.

Model 1 represents an atmospheric model which behaves essentially as a black body, both in X-ray absorption and optical emission. Model 2 represents an optically thick atmosphere to the incident X-rays but is optically thin for the emitted visible light. A soft X-ray flux which

would be absorbed high in the photosphere of HZ Her would have this characteristic. Model 3 approximates the case where hard X-rays penetrate deeply into the atmosphere of HZ Her and only the outer part of this stimulated region can contribute to optical pulsations.

Now write $L(t,\rho)$ in terms of the intrinsic X-ray beam L_x and a surface pulsation attenuation factor A

$$L(t,\rho) = L_x\left(\phi_{apparent}(t),\hat{\rho}\right)A(t_c)$$

where

$$\phi_{apparent} = \omega_p'(t - t_1 - t_2) + \phi_1 + \phi_2$$

$\omega_p' = \omega_p - e\omega_b$

ω_p = pulsar angular frequency

ω_b = binary angular frequency

e = +1 if pulsar spin is prograde

= -1 if pulsar spin is retrograde

$t_1 = \frac{1}{c}\left\{[x\cos(\omega_b t + \phi_o) - y\sin(\omega_b t + \phi_o)]\sin i - z\cos i\right\}$

= time delay from the surface element ds to the observer

t_2 = ρ/c = time delay from Her X-1 to the HZ Her surface element

ϕ_o = the binary phase at t = 0 (in radians)

t_c = time constant for absorption-remission processes at ds

$\phi_1 = -\tan^{-1}\omega_p' t_c$ = phase shift due to the atmospheric constant t_c

and $\phi_2 = e\tan^{-1} y/(d-x)$ = phase angle between the mass axis and the surface element as seen from Her X-1 .

We have introduced an attenuation factor $A(t_c)$ to represent the reduction in pulsation amplitude caused by finite reprocessing times

($t_c \gtrsim 1$ sec). We have assumed a very simple form resulting from an exponential cooling curve (see e.g., Avni and Bahcall 1974)

$$A(t_c) = [1 + (\omega_p' t_c)^2]^{-\frac{1}{2}} \tag{11}$$

For t_c equal to a constant over the surface, this only causes an overall scale factor, but when t_c varies over the surface, other effects can be produced. It is not evident what variation in reprocessing times, if any, will occur over the surface. To study the possible effects of any variations in cooling time we have varied the cooling time over the surface according to

$$t_c = t_o + \Delta t\ \theta_{HZ\ Her} \tag{12}$$

where t_o = cooling time at the surface point on the mass axis

$\theta_{HZ\ Her}$ = angle from the mass axis to the surface element from the center-of-mass of HZ Her

Δt = range of cooling times .

A variety of parameters were tried, with t_o and Δt varying from 0 to 20 seconds. Our "basic" models have $\Delta t = 0$.

We have assumed that the X-ray flux could be expressed as

$$L_x(\phi,\hat{\rho}) = L_x^o\ f_1(\phi(t)) f_2(\hat{\rho}) \tag{13}$$

where L_x^o = the equatorial X-ray flux

$f_1(\phi(t)) = 1 + \cos\phi$

$f_2(\hat{\rho}) = |\hat{\rho} \times \hat{e}_z|^2$

This value of f_2 makes the X-ray flux almost independent of polar angle for the relatively small angle that HZ Her subtends.

While a simple form has been given to f_1, a more complex periodic beam structure could have been used without appreciably changing any results. A more complex azimuthal beam shape simply produces harmonics of the basic frequency ω_p'. The geometrical factors plus attenuation factors serve to greatly diminish any such harmonic components relative to the fundamental, so only the fundamental frequency is expected to be visible. In fact, no significant harmonics are seen in the optical data and little in the X-ray data.

The polar angle dependence f_2 has been varied for some models. In addition to the standard $|\hat{\rho} \times \hat{e}_z|^2$ dependence, an X-ray fan beam was used with characteristic angles above and below the orbital plane of ± 0.05 radians and ± 0.10 radians. f_2 was essentially constant within these angles and zero outside of them. These are denoted EB (equatorial beam). Complementary cases with no X-ray flux within this region, called ES (equatorial shadow) were also tried.

Having numerically generated I(t) for some nominal time interval (e.g., 2.91 h = 0.071 cycles), we can then analyze this function exactly as the actual data; i.e., Fourier transform and signal average the function. This procedure was followed for all binary phases and for different variations of Models 1, 2 and 3.

Before describing the detailed results of these calculations, we will attempt to develop some qualitative idea of what this model might yield with the following interfering wave analogy. The 1.24 s pulse period establishes "waves" with a 1.24 light second wavelength in the system. The distance to the CM from Her X-1 is about 11 wavelengths, so the HZ Her surface is fairly large on the scale of this wavelength. In the model, reprocessing occurs on the surface, so HZ Her acts in many ways as a "mirror" for the

1.24 light second wave fronts. For example, if HZ Her were a filled Roche lobe, it would be pointed towards Her X-1 and thus at phase 0.5 one would be unable to see an "image" of the source off the pointed mirror. Consequently we would not expect to see pulsations (1.24 second) at this phase *if* the Roche lobe were filled. Similarly, at phases .25 and .75 one might expect to see rather strong "reflections" off the gently curved sides of a filled Roche lobe.

One would also expect the Her X-1 pulsar frequency to be doppler shifted by the velocity with respect to the cm of the "reflecting" region. Thus an observer fixed anywhere in the binary system would see the same pulsar frequency; however, an outside observer would see a frequency shifted by the component of the velocity towards her. The velocity of this region is proportional to the distance from the center of mass to the filled Roche surface and this distance depends on the mass ratio. While this intuitive optical analogy need not describe the actual model behavior with great precision, it does give a feeling for the results of the detailed calculation, and hopefully from the real system as well.

The model calculations for each set of assumptions are shown in two ways. First we discuss the predicted amplitude of pulsation as a function of binary phase; secondly we show the pulsation frequency (or doppler shift velocity) as a function of binary phase and mass ratio.

The resultant amplitude profiles for Models 1, 2 and 3 using the *critical* Roche surface and $R = 1.65$ with $i = 90°$ are shown in Figure 7 with the data from Figure 2(b) displayed below them. The curves have been plotted on a log scale so their shapes are directly comparable. These shapes have been found to be very insensitive to variations in either R or i. The difference in the peak heights of the data near phases 0.25

and 0.75 may be due to differing 35-day phase sampling for Features I and II.

All three models show good consistency with the data between orbital phases 0.25 and 0.75. In particular the peak to valley ratio produced by the models is consistent with the data. Outside this region Models 2 and 3 appear to give excessively large pulsation amplitudes. In spite of this difficulty, we accept Models 2 and 3 as possible descriptions, mainly because the effects of a proper treatment of the 35-day cycle are not known.

To decide which Roche equipotential contour HZ Her may fill, we plot in Figure 8 three Model 1 amplitude profiles corresponding to the different contours. The right hand side of the figure shows the three trial contours labeled by their maximum extent from the center of mass of HZ Her along the mass axis toward Her X-1. The critical Roche surface defines 100% for this extent. Any surface larger than this would have the saddle point (the inner Lagrangian point) in its interior which would result in large mass transfer from HZ Her to Her X-1. The three corresponding amplitude profiles are plotted on the left hand side of the figure.

Comparison of the Figure 8 profiles with the data profile in Figure 2(b) indicates that only the critical Roche contour produces a sufficiently low optical pulsation amplitude near orbital phase 0.5. Qualitatively, this indicates that the surface of HZ Her must be *pointed*, not rounded. It is difficult for material in any tidal lobe to form such a point. If somehow, the material did occupy such a point, HZ Her would deviate so strongly from sphericity that tidal torques would force the star to corotate. Consequently a critical tidal lobe is extremely unlikely. We conclude that HZ Her corotates and essentially fills its critical Roche lobe. This

analysis of the pulsation amplitude clearly supports the first assumption of the model.

Another important aspect of the pulsation amplitude results concerns the normalization. Using Model 1 we now investigate how much the geometrical averaging over the surface degrades the reflection effect for the optical pulsations, and compare it with the data.

The time-averaged reflection effect as a function of binary phase calculated for the critical Roche lobe is shown in Figure 9(a). This curve rises to a maximum of just over 3% of the value used for the X-ray luminosity. This maximum is simply the apparent solid angle of HZ Her as seen by Her X-1. Figure 9(b) shows the pulsed reflection profile calculated with Model 1 and a critical Roche surface for comparison. This curve has a maximum corresponding to about 0.17% of the X-ray luminosity defined above. As a fraction of the maximum of the top curve, the optical pulsation maximum is about 5%. Since we define our experimental pulsed fraction this way, i.e., with a maximum light from HZ Her, we see that the observed pulse fraction of 0.2% as seen in Figure 5(a) is lower than the model prediction by a factor of 25.

While we have no detailed explanation for this factor of 25 in the pulsation strength, it seems likely that it measures the intrinsic efficiency of the atmosphere for reprocessing the X-ray pulses into optical pulses. There seem to be at least two mechanisms would could produce pulses with this low efficiency.

First, pulses caused by the heating and cooling of HZ Her will be attenuated by the long timescale of the reprocessing of the X-ray energy. As mentioned in the introduction, it is expected that the cooling time t_c will be $\sim$ 1 - 10 seconds. Using equation (11) defined for the model calcu-

lations, one obtains an attenuation factor of 25 with $t_c \simeq 5s$. One can also obtain this attenuation factor with a wide variety of surface position dependent time scale models as exemplified by equation (12).

A second possible mechanism for pulsations is that discussed in Paper III; the conversion of a small amount of the X-ray energy into optical quanta by photoionization and line emission after recombination. Since this process occurs on a short timescale, the amplitude of these pulsations is simply the ratio of the emission photon energy to the incident X-ray photon energy times the geometrical efficiency. Assuming 3 eV for the visible photon, 1 keV for the average X-ray and a geometrical efficiency from Figure 9(b) of 0.0017, we expect the ratio of fluxes to be

$$F_{\text{optical}}^{\text{pulsed}} / F_{\text{X-ray}} \sim 5 \times 10^{-6}$$

Experimentally,

$$F_{\text{X-ray}} \sim 2 \times 10^{-8} \text{ ergs cm}^{-2}\text{s}^{-1}$$

(Tannenbaum et al 1972; Giacconi et al 1973; Shulman et al 1975) so we expect

$$F_{\text{optical}}^{\text{pulsed}} \sim 1 \times 10^{-13} \text{ ergs cm}^{-2}\text{s}^{-1}.$$

We actually see about 2×10^{-13} ergs cm^{-2} s^{-1} so the observed flux and the model calculation are consistent with this alternative pulsation mechanism.

Since neither the cooling time within nor the X-ray spectrum incident upon HZ Her's atmosphere is known precisely, we cannot predict, a priori, the relative contributions of the two reprocessing mechanisms to the total amount of 1.24 s optical pulsation in regions I and II.

Figure 9(c) shows the fraction of the optical flux which the model predicts should appear pulsed (it should be noted that the model calculations completely ignore the optical flux generated by the thermonuclear reactions in HZ Her). Pulses produced by long time constant heating will give far less than this amount, but pulsations in emission lines produced by the

above mechanism should give essentially this fraction. The emission line pulsation data described in Paper III in fact appear consistent with this.

We now turn to the question of the pulsed frequency predicted by the models, and compare this with the data. Figure 10 shows five such frequency profiles calculated (Model 1) for several values of R at $i = 90°$ and plotted with the significant detections of Features I and II.

First, note the profiles intersect below the $v = 0$ line at orbital phase 0.5. This is because prograde rotation was assumed (see equation 10, $e = +1$). The hypothesis of prograde pulsar spin can be checked against the average velocities for Features I and II. The unweighted average between the $+16.9 \pm 0.6$ km s^{-1} value for Feature I and the -24.2 ± 1.0 km s^{-1} value for Feature II is equal to -3.65 ± 0.6 km s^{-1}. The model calculations indicate that this average should be -3.55 km s^{-1} — in very good agreement with the data (retrograde spin would predict $+3.55$ km s^{-1}). Thus the spin angular momentum of Her X-1 is aligned to the orbital angular momentum of the binary system to within 46° as derived from the (formal) 2σ error in the data.

Returning to the question of mass ratio, Figure 10 indicates that the mass ratio, R, lies between 1.5 and 2.0. These curves are virtually independent of i (we keep vsini = 169 km s^{-1}). Furthermore, once the sense of the pulsar spin is known and the model is chosen, a unique mass ratio can be assigned to each data point in Figure 10. These mass ratios are plotted vs Julian data in Figure 4(b) for Model 1 and listed in the last column of Table 3.

Although no systematic difference between the data from Region I and Region II is evident, it is apparent that the scatter in the data exceeds expectations based on the stated errors. This is also seen in

Figure 4(a), but as pointed out before, the residuals from Region III indicate the (statistical) error assignments are reasonable. None of our model variations appreciably alter the amount of scatter. We are forced to the conclusion that some additional process is (randomly) doppler shifting the pulsations a small amount. We assume this adds *only* scatter to the data. For the 21 points, we typically find $\chi^2 \sim 100$ after fitting with a model because of this scatter.

We have made calculations with a number of variations on Models 1, 2 and 3. In most respects the results are model independent, but to determine the exact mass ratio we must study these variations quantitatively, not just qualitatively. For each model variation, we have varied R to optimize the fit to the data. Essentially all models will fit the velocity data with an appropriate mass ratio, but models differed substantially in their predicted amplitude profile as a function of binary phase. As stated earlier, we consider the observed absence of pulsations at $\phi = 0.5$ to be a critical test for any model. Table 4 shows the models used and the mass ratio derived. Column 1 lists the model number and column 2 gives the orbital inclination. The X-ray beam shape in polar angle has also been varied. Column 3 describes the X-ray illumination assumed. As mentioned earlier, ES and EB mean an equatorial shadow and equatorial X-ray beam respectively. Their half widths in radians as subtended from Her X-1 are stated. Column 5 indicates the model acceptability on the basis of the amplitude profile.

To study possible biases in the mass ratio measurement caused by any surface position dependent cooling times, we have used equation (12) with Model 1. A very wide range of cooling times was tested and these parameters are defined in columns 6 and 7. Surprisingly, any variations

that strongly altered the mass ratio also produced amplitude profiles quite inconsistent with the data. Those tests producing an attenuation factor between 6 and 60 are shown and the attenuation factor is given in column 8. The family of models with very rapid cooling times at the inner Lagrangian point are the only set which change R appreciably, but these give either insufficient attenuation or an unacceptable amplitude profile.

The mass ratio values in Table 4 for differing inclinations of otherwise identical models are essentially constant. The results of the model study of Features I and II therefore directly establish the mass ratio of the HZ Her - Her X-1 system. The appropriate errors on the mass ratio can be determined after consideration of the contributing factors. These factors are, in order of increasing importance:

1. The formal statistical errors of the data, which amount to a variation in mass ratio of only ± 0.01 out of 1.65.
2. The model-dependent systematic variations. As can be seen in Table 4, the different models and their variations only slightly alter the mass ratio. Thus, even without determining the best model, we can estimate the mass ratio error produced by using a non-optimal model.
3. The scatter of unknown origin in the data points as shown in Figure 10.

To attempt to minimize the error introduced by the model dependent systematics of factor 2, the central value of R is raised from the Model 1 value of 1.64 to 1.68 with an estimated systematic error of ~ 0.05. The possible consequences of factor 3 are more difficult to estimate because of the unknown origin of the scatter in the data. To be conservative we arbitrarily double the size of the model-independent errors to ± 0.10 — an

order of magnitude larger than the formal statistical errors.

The masses of the system can now be determined with the value established above for the mass ratio R, the knowledge that HZ Her occupies its critical Roche surface, and with the X-ray eclipse duration of 0.24 ± 0.01 days from Giacconi et al (1973).

For a binary system with a filled Roche lobe star and a specified eclipse duration, the mass ratio and the orbital inclinations are related. As the inclincation angle decreases, the relative size of the Roche lobe-filling star, and thus the mass ratio, must increase to maintain a constant eclipse duration. The curve of R vs i for the critical Roche surface subtending an eclipse half angle of 25.4° has been calculated with a technique similar to that described by Chanan, Middleditch and Nelson (1975). In Figure 11 this curve is shown together with the almost flat curve for R derived from the optical pulsation data.

The region of intersection of the two curves limits the orbital inclination to values above 84°. With the value for the mass function for the Her X-1 system, $m = 0.853(2)M_{\odot}$ established by Tananbaum et al (1972), the mass of Her X-1 may be expressed as

$$M_{HerX-1} = m \sin^{-3} i \, R^{-1}(1 + 1/R)^2$$

and the mass of the companion, HZ Her is given by

$$M_{HZHer} = R \, M_{HerX-1} .$$

Accounting for the variation of $\sin^{-3} i$ over the common area of the two regions on the i-R plane, the values for the masses of the two components of the system are given by

$$M_{HerX-1} = 1.30 \pm 0.14\ M_{\odot}$$

$$M_{HZHer} = 2.18 \pm 0.11\ M_{\odot}$$

The evidence that Her X-1 is a neutron star is overwhelming. The mass found here is well within the range expected for neutron stars, but it is above the Chandrasekhar limit for white dwarfs and below the ranges of masses generally expected for Black Holes. The relatively fast and stable period of pulsations (see Giacconi 1975) along with its mass make the identification a virtual certainty. The data and arguments given above represent the first accurate measurement of the mass of a neutron star.

b) Region III — Constraints on Disk Models

Pulsations seen in Region III can help define the nature of the Her X-1 region. We believe these pulsations originate from a cloud of gas where the gas stream and accretion disk collide. The 35-day behavior of these pulses as shown in Figure 5(c) suggests they are related to the X-ray dips seen at similar binary phase and presumably caused by gas at the stream-disk intersection point (see e.g., Pines, Pethick and Lamb 1973). The pulsations are greatest at binary phase ~ 0.86.

The thickness of such a cloud along the line of sight will determine the degree of pulsations expected in the opposite direction ($\phi \sim 0.36$) from simple optical arguments. Our limit for these pulsations is less than 0.2 of those seen in Region III. This produces a lower limit for the cloud thickness of 1.5×10^{10} cm. The typical duration of pulsations (~ 3 h) establishes a minimum width for such a cloud as $\sim 9 \times 10^{10}$ cm by simple diffraction arguments. Finally, assuming the stream trajectory is known

(see Lubow and Shu 1975), the radius of the disk can be estimated from the mean phase of these pulsations to be $\sim 1 \times 10^{11}$ cm. A more detailed analysis of this feature can be found in Middleditch (1975).

V. CONCLUSIONS

Our extensive optical observations of HZ Her have revealed weak, intermittent pulsations at frequencies very near to, but in general not identical to, the expected Her X-1 frequency. These pulsations show correlations with the binary phase and three distinct regions of pulsation in frequency-binary phase space have been discovered (labeled I, II and III). The first two regions are associated with the actual surface of HZ Her, while the third is associated with the area immediately surrounding Her X-1. Surprisingly, these regions each show definite (and different) correlations with the 35-day cycle of the system. We cannot yet account for these correlations, but note that very similar behavior (to Regions I and II) exists in the photometric data of Deeter et al (1975).

We have constructed a simple geometrical model of the system to explain the pulsations of Regions I and II. The model simply calculates the travel time from Her X-1 to a point on HZ Her and then to the observer with the consequent pulsar frequency phase shift. The integration over the surface of HZ Her is then performed. The intensity as a function of time is finally tabulated, and this is reduced in a fashion similar to the data reduction. A variety of X-ray beam profiles and reemission mechanisms were tested. These were found to have little effect on the results. For any assumed equipotential surface of HZ Her, mass ratio and orbital inclination, we can calculate the expected amplitude and frequency of pulsation as a function of binary phase.

By comparing these calculations with the data, we have concluded that:

- The surface of HZ Her is pointed towards Her X-1.
- HZ Her fills its Roche lobe (and thus must be corotating with the orbital motion).
- Her X-1's spin is prograde (the same sense as the orbital motion)
- The mass ratio is $M_{HZHer} / M_{HerX-1} = 1.68 \pm 0.10$
- $M_{HerX-1} = 1.30 \pm 0.14\ M_{\odot}$
- $M_{HZHer} = 2.18 \pm 0.11\ M_{\odot}$
- $i = 87° \pm 3°$

While the model appears quite consistent with the data, the surface phenomena of HZ Her are not sufficiently well known for us to predict the actual amplitude of pulsation expected. Fortunately, the wide variations in surface behavior tested showed that the results are quite insensitive to the assumed surface behavior. Additionally, the model is unable to predict any of the observed 35-day behavior. It is our opinion, based upon the wide variety of models studied, that a more complete model would not substantially alter our results.

The existence of optical pulsations and their binary phase from Region III can constrain models of the disk around Her X-1. We estimate the radius of such a disk to be 10^{11} cm.

ACKNOWLEDGMENTS

We are extremely grateful for many discussions with Gary Chanan and Terry Mast concerning the interpretation and presentation of the data. Such an extensive observing program was only possible with the able help of Chris Sunzeri who performed the majority of observations. We also wish to thank Tim Daly for the excellent drawings. Finally we wish to thank David Pines for his encouragement of this project.

This work was done under the auspices of the U. S. Energy Research and Development Administration.

REFERENCES

Alme, M. L., and Wilson, J. R. 1974, Ap. J., 194, 147.

Avni, Y., and Bahcall, J. N. 1974, Ap. J., 191, 221.

Bahcall, J. N., and Bahcall, N. A. 1972, Ap. J. (Letters), 178, L1.

Basko, M. M., and Sunyaev, R. A. 1973, Ap. & Space Sci., 23, 117.

Boynton, P., private communication.

Chanan, G., Middleditch, J., and Nelson, J. 1975, preprint submitted to the Astrophysical Journal (LBL Report No. 4290).

Cocke, W. J., Hintzen, P., Scott, J. S., and Worden, S. P. 1973, Nature Phys. Sci., 244, 137.

Dahab, R. E. 1974, Ap. J., 187, 351.

Davidsen, A., Henry, J. P., Middleditch, J., and Smith, H. E. 1972, Ap. J. (Letters), 177, L97.

Davidsen, A., Margon, B., and Middleditch, J. 1975, Ap. J., 198, 653.

Davison, P. J. N., and Fabian, A. C. 1974, M.N.R.A.S., 169, 27p.

Deeter, J., Crosa, L., Gerend, D., and Boynton, P. 1975, preprint submitted to the Astrophysical Journal.

Forman, W., Jones, C. A., and Liller, W. 1972, Ap. J. (Letters), 177, L103.

Frolich, A. 1973, Ap. Letters, 13, 233.

Giacconi, R. 1975, in Astrophysics and Gravitation, Proceedings of the Sixteenth Annual Solvay Conference on Physics, The Solvay Foundation (L'Université de Bruxelles), p. 27.

Giacconi, R., Gursky, H., Kellogg, E., Levinson, R., Schreier, E., and Tananbaum, H. 1973, Ap. J., 184, 227.

Grandi, S. A., Hintzen, P. M. N. O., Jensen, E. B., Rydgren, A. E., Scott, J. S., Stickney, P. M., Whelan, J. A. J., and Worden, S. P. 1974, Ap. J., 190, 365.

Groth, E. J. 1974, Ap. J., 192, 517.

Groth, E. J., and Nelson, M. R. 1972, Ap. J. (Letters), 178, L111.

Lubow, S., and Shu, F. H. 1975, Ap. J., 198, 383.

McClintock, J. E., Clark, G. W., Lewin, W. H. G., Schnopper, H. W., Canizares, C. R., and Sprott, G. F. 1974, Ap. J., 188, 159.

Middleditch, J. 1975, Ph.D. Thesis, LBL Report No. 3639.

Middleditch, J., and Nelson, J., 1973, Ap. Letters, 14, 129.

Pines, D., Pethick, C. J., and Lamb, F. K. 1973, Talk presented at the Sixth Texas Symposium on Relativistic Astrophysics (published in the Annals of the New York Academy of Sciences as Part of the Symposium Proceedings, Vol. 224, p. 237).

Shulman, S., Friedman, H., Fritz, G., and Yentis, D. 1975, Ap. J. (Letters), 174, 143.

Tananbaum, H., Gursky, H., Kellogg, E. M., Levinson, R., Schreier, E., and Giacconi, R. 1972, Ap. J. (Letters), 174, 143.

TABLE 1. "Turn-on" epochs.

Interval Number	Start of Interval (0.0 cycles) (JD-2,440,000.5)	"Turn-on" (JD-2,440,000.5)	Turn-on phase (binary cycles)	Interval gap (cycles)
1	1488.89	1501.18	7.23	21
2	1524.59	1535.95	6.68	21
3	1560.30	1571.65	6.68	20
4	1594.30	1606.59	7.23	20
5	1628.30	1639.68	6.68	20
6	1662.31	1674.60	7.23	20
7	1696.31	1708.60	7.23	20
8	1730.31	1742.60	7.23	21
9	1766.02	1778.31	7.23	21
10	1801.72	1814.01	7.23	21
11	1837.42	1848.78	6.68	20
12	1871.43	1883.72	7.23	21
13	1907.13	1918.49	6.68	20
14	1941.13	1953.43	7.23	21
15	1976.84	1988.19	6.68	20
16	2010.84	2023.13	7.23	21
17	2046.54	2057.90	6.68	20
18	2080.55	2092.84	7.23	21
19	2116.25	2127.61	6.68	20
20	2150.25	2162.54	7.23	21
21	2185.96	2197.31	7.23	21
22	2221.66	2233.02	6.68	20
23	2255.66	2267.95	7.23	21
24	2291.37	2303.72	6.68	20
25	2325.37	2337.66	7.23	—

TABLE 2. HZ Her run data.

Run Number	Date of Run	Run Center JD -2,440,000.5	35-Day Phase (binary cycles)	Run length (phase)	Run length (hours)
1	21Jul72	1519.320	17.898	.139	5.65
2	22Jul72	1520.278	18.462	.074	3.02
3	28Jul72	1526.248	.973	.032	1.29
4	3Aug72	1532.270	4.515	.072	2.94
5	4Aug72	1533.286	5.113	.072	2.94
6	5Aug72	1534.276	5.695	.072	2.94
7	6Aug72	1535.276	6.283	.072	2.94
8	7Aug72	1536.286	6.877	.072	2.92
10	11Aug72	1540.295	9.235	.108	4.40
11	16Aug72	1545.333	12.199	.072	2.94
12	18Aug72	1547.222	13.310	.037	1.50
13	21Aug72	1550.309	15.126	.036	1.48
15	24Aug72	1553.250	16.855	.072	2.95
18	2Sep72	1562.270	1.161	.109	4.45
20	9Sep72	1569.230	5.254	.085	3.45
21	13Sep72	1573.216	7.599	.037	1.50
22	14Sep72	1574.239	8.201	.110	4.50
23	20Sep72	1580.235	11.727	.105	4.30
24	21Sep72	1581.163	12.273	.048	1.95
25	27Jan73	1709.506	7.762	.041	1.66
26	19Feb73	1732.507	1.291	.075	3.04
27	10Mar73	1751.480	12.450	.074	3.00
28	7Apr73	1779.421	7.884	.082	3.33
29	9Apr73	1781.453	9.079	.089	3.65
30	11Apr73	1783.440	10.248	.099	4.02
31	12Apr73	1784.435	10.834	.101	4.12
32	21Apr73	1793.343	16.073	.084	3.42
33	22Apr73	1794.410	16.701	.129	5.26
34	26Apr73	1798.392	19.043	.140	5.69
35	27Apr73	1799.389	19.629	.136	5.56
36	29Apr73	1801.401	20.813	.110	4.48
37	30Apr73	1802.361	.378	.137	5.56
38	8May73	1810.371	5.089	.152	6.20
39	10May73	1812.353	6.254	.151	6.15
40	11May73	1813.358	6.846	.141	5.73
41	12May73	1814.363	7.437	.146	5.96
42	13May73	1815.359	8.023	.143	5.82
43	15May73	1817.348	9.192	.072	2.92
44	16May73	1818.421	9.824	.088	3.59
45	17May73	1819.268	10.322	.079	3.23
46	21May73	1823.353	12.724	.140	5.73
47	22May73	1824.306	13.285	.099	4.03
48	23May73	1825.343	13.895	.147	5.99
49	8Jun73	1841.335	2.301	.146	5.94
50	11Jun73	1844.330	4.063	.091	3.71

TABLE 2. (continued)

Run Number	Date of Run	Run Center JD -2,440,000.5	35-Day Phase (binary cycles)	Run length (phase)	Run length (hours)
51	12Jun73	1845.292	4.628	.083	3.39
52	13Jun73	1846.355	5.254	.137	5.57
53	20Jun73	1853.341	9.363	.141	5.76
54	21Jun73	1854.409	9.991	.085	3.45
55	22Jun73	1855.304	10.518	.061	2.49
56	23Jun73	1856.340	11.127	.144	5.87
58	25Jun73	1858.351	12.310	.149	6.08
59	3Jul73	1866.353	17.016	.144	5.85
60	8Jul73	1871.369	19.967	.142	5.80
61	9Jul73	1872.348	.542	.146	5.95
62	10Jul73	1873.345	1.129	.157	6.39
63	17Jul73	1880.345	5.246	.154	6.29
64	18Jul73	1881.328	5.824	.139	5.67
65	20Jul73	1883.372	7.026	.105	4.27
66	21Jul73	1884.310	7.578	.126	5.13
67	22Jul73	1885.362	8.197	.117	4.75
68	25Jul73	1888.326	9.940	.145	5.90
69	26Jul73	1889.331	10.531	.155	6.30
70	30Jul73	1893.317	12.876	.143	5.83
71	3Aug73	1897.328	15.235	.115	4.68
72	4Aug73	1898.312	15.814	.142	5.78
73	5Aug73	1899.286	16.387	.111	4.53
74	8Aug73	1902.360	18.195	.076	3.08
75	9Aug73	1903.288	18.740	.116	4.72
76	15Aug73	1909.289	1.270	.124	5.04
77	19Aug73	1913.282	3.619	.123	5.03
78	20Aug73	1914.281	4.206	.118	4.80
79	21Aug73	1915.280	4.794	.125	5.08
80	23Aug73	1917.264	5.961	.116	4.73
81	24Aug73	1918.288	6.563	.090	3.69
82	28Aug73	1922.261	8.900	.116	4.73
83	29Aug73	1923.255	9.485	.119	4.85
84	30Aug73	1924.258	10.075	.112	4.56
85	1Sep73	1926.254	11.249	.112	4.56
86	2Sep73	1927.252	11.836	.109	4.46
87	3Sep73	1928.247	12.421	.112	4.56
88	4Sep73	1929.263	13.018	.088	3.59
89	6Sep73	1931.242	14.183	.107	4.34
90	18Sep73	1943.224	1.230	.098	4.00
91	19Sep73	1944.200	1.804	.078	3.17
92	20Sep73	1945.200	2.393	.079	3.20
93	19Mar74	2125.424	5.397	.123	5.01
94	20Mar74	2126.432	5.989	.123	5.00
95	21Apr74	2158.411	4.799	.119	4.86
96	22Apr74	2159.379	5.368	.149	6.07
97	1May74	2168.261	10.593	.032	1.30

TABLE 2. (continued)

Run Number	Date of Run	Run Center JD -2,440,000.5	35-Day Phase (binary cycles)	Run length (phase)	Run length (hours)
98	2May74	2169.357	11.237	.148	6.04
99	3May74	2170.387	11.843	.133	5.44
100	4May74	2171.426	12.454	.090	3.66
101	11May74	2178.328	16.514	.098	3.98
102	20May74	2187.368	.831	.136	5.55
103	26May74	2193.346	4.347	.127	5.16
104	9Jun74	2207.339	12.577	.157	6.38
105	17Jun74	2215.274	17.245	.074	3.03
106	26Jun74	2224.326	1.569	.156	6.36
107	27Jun74	2225.324	2.156	.134	5.44
108	3Jul74	2231.338	5.693	.166	6.79
109	4Jul74	2232.349	6.287	.157	6.39
110	5Jul74	2233.339	6.870	.163	6.66
111	21Jul74	2249.330	16.275	.153	6.25
112	22Jul74	2250.332	16.865	.147	5.98
113	4Aug74	2263.247	4.461	.024	.98
114	5Aug74	2264.303	5.082	.126	5.12
115	6Aug74	2265.303	5.671	.123	5.00
116	7Aug74	2266.316	6.267	.113	4.60
117	13Aug74	2272.287	9.778	.128	5.23
118	21Aug74	2280.281	14.480	.110	4.49
119	23Aug74	2282.269	15.650	.117	4.77
120	24Aug74	2283.267	16.236	.116	4.71
121	25Aug74	2284.245	16.812	.090	3.68
122	5Sep74	2295.252	2,286	.094	3.84
123	6Sep74	2296.242	2.868	.103	4.20
124	7Sep74	2297.244	3.458	.096	3.92
125	10Sep74	2300.247	5.224	.098	3.99
126	11Sep74	2301.237	5.806	.106	4.33

TABLE 3. Parameters of significant events.

Run	Calendar Date UTC.	Run Center JD -2,440,000.5	35-Day Phase (binary cycles)	Run length (days)	Run length (cycles)	Barycentric frequency (Hertz)	Derivative of frequency $\times 10^9$ (Hertz s^{-1})	Power in Feature	Region Number	Model 1 Mass Ratio
5	4Aug72	1533.317	5.131	.061	.036	.808014(22)	-2.8(30.3)	13.2	--	
7	6Aug72	1535.275	6.283	.121	.071	.807924(9)	-3.3(6.8)	15.8	I	1.59(0.07)
10	11Aug72	1540.234	9.199	.061	.036	.808407(22)	+5.1(30.7)	13.5	--	
20	9Sep72	1569.219	5.248	.121	.071	.807910(8)	+4.5 (6.2)	23.0	I	1.55(0.065)
31	12Apr73	1784.410	10.819	.121	.071	.807457(10)	+1.7 (8.4)	12.5	III	
36	29Apr73	1801.402	20.813	.187	.110	.807437(6)	+1.0 (4.1)	17.5	III	
39	10May73	1812.347	6.250	.243	.143	.807917(4)	+0.0 (1.7)	22.6	I	1.57(0.035)
44	16May73	1818.422	9.824	.150	.088	.807459(9)	-6.7 (5.4)	12.5	III	
46	21May73	1823.408	12.756	.121	.071	.807845(10)	+3.5 (4.8)	15.0	II	1.39(0.065)
48	23May73	1825.279	13.857	.121	.071	.807752(11)	-3.3 (8.1)	11.6	II	2.29(+0.26,-0.22)
52	13Jun73	1846.355	5.254	.232	.137	.807918(3)	-0.7 (1.4)	36.4	I	1.57(0.03)
63	17Jul73	1880.275	5.204	.121	.071	.807924(6)	+9.9 (5.3)	32.3	I	1.75(0.05)
68	25Jul73	1888.264	9.903	.121	.071	.807608(8)	+18.9 (5.8)	27.6	III	
70	30Jul73	1893.265	12.845	.139	.082	.807807(9)	-7.7 (4.9)	19.6	II	1.635(0.105)
71	3Aug73	1897.291	15.213	.121	.071	.807941(9)	-15.2 (7.3)	17.0	I	1.90(0.08)
72	4Aug73	1898.276	15.792	.167	.098	.807798(6)	0.0 (3.2)	21.4	II	1.76(0.05)
78	20Aug73	1914.281	4.206	.200	.118	.807944(6)	+8.2 (3.7)	14.0	I	1.90(0.08)
79	21Aug73	1915.235	4.767	.121	.071	.807813(9)	-5.5 (7.4)	17.9	II	1.62(0.06)
82	28Aug73	1922.224	8.878	.121	.071	.807556(9)	+11.9 (6.8)	19.2	III	
82	28Aug73	1922.224	8.878	.121	.071	.807814(11)	+13.8 (8.6)	12.4	II	1.47(+0.14,-0.11)
86	2Sep73	1927.220	11.817	.121	.071	.807840(10)	-7.4 (7.9)	13.3	II	1.445(+0.085,-0.075)
91	19Sep73	1944.201	1.804	.132	.078	.807819(12)	-4.2 (6.7)	11.8	II	1.62(0.09)
95	21Apr74	2158.412	4.799	.203	.119	.807808(5)	-3.9 (2.4)	19.7	II	1.67(0.045)
109	4Jul74	2232.276	6.245	.121	.071	.807904(8)	-6.4 (5.8)	23.5	I	1.51(0.05)
110	5Jul74	2233.343	6.872	.133	.078	.807551(9)	+14.8 (6.4)	18.1	III	
111	21Jul74	2249.292	16.253	.185	.109	.807901(9)	-3.6 (2.2)	32.4	I	1.46(0.055)
116	7Aug74	2266.282	6.246	.121	.071	.807917(6)	-1.5 (4.8)	32.8	I	1.605(0.045)
120	24Aug74	2283.267	16.236	.196	.116	.807913(5)	-1.6 (2.4)	19.2	I	1.58(0.04)
125	10Sep74	2300.238	5.218	.148	.087	.807920(4)	+3.4 (3.1)	38.7	I	1.71(0.04)

TABLE 4. Model HZ Her/Her X-1 mass ratios.

Model Number	Orbital Inclination	Illumination Pattern	Mass Ratio R	Amplitude Profile Acceptability*	Cooling at L1 t_o	Cooling Time Range Δt	Amplitude Attenuation Factor
1	90°	full	1.64	yes	0	0	1
1	75°	full	1.63	yes	0	0	1
1	60°	full	1.64	yes	0	0	1
1	45°	full	1.64	yes	0	0	1
1	30°	full	1.66	marginal	0	0	1
2	90°	full	1.67	yes	0	0	1
2	75°	full	1.67	yes	0	0	1
3	90°	full	1.66	yes	0	0	1
3	75°	full	1.67	yes	0	0	1
1	90°	0.05ES†	1.66	marginal	0	0	1
1	75°	0.05ES	1.70	no	0	0	1
2	90°	0.05ES	1.70	yes	0	0	1
2	75°	0.05ES	1.78	no	0	0	1
3	90°	0.05ES	1.70	marginal	0	0	1
3	75°	0.05ES	1.71	marginal	0	0	1
1	90°	0.10ES	1.71	no	0	0	1
1	75°	0.10ES	1.73	marginal	0	0	1
1	90°	0.05EB†	1.65	marginal	0	0	1
1	75°	0.05EB	1.58	marginal	0	0	1
1	90°	0.10EB	1.68	yes	0	0	1
1	75°	0.10EB	1.60	yes	0	0	1
1	90°	full	1.65	yes	8	-6	34
1	90°	full	1.60	yes	2	+6	16
1	90°	full	2.0	no	10	-10	32
1	90°	full	1.4	yes	0	+10	6
1	90°	full	1.4	no	0	+20	12
1	90°	full	1.52	marginal	1	+14	16
1	90°	full	1.66	yes	15	-14	60
1	90°	full	1.65	yes	8	-7	32

*Acceptability requires a minimum peak to valley ratio of 5 [as derived from the observations shown in Figure 2(b)] in the model amplitude profiles between the ϕ = 0.25, 0.75 values and the ϕ = 0.5 value for the orbital phase.

†ES and EB designate the X-ray illumination patterns on the lobe of HZ Her which include an equatorial shadow or consist of an equatorial band respectively. The numbers immediately preceding the designations give the half-widths of the shadow or band in radians as seen from Her X-1.

FIGURE CAPTIONS

Fig. 1. (a,b) Detailed sections of power spectra near the Her X-1 frequency from data taken on two nights showing the three typical types of optical pulsation. The circles in the upper centers of the frames indicate the motion of Her X-1 during the run. The doppler shifted X-ray pulse frequency is given by the projection of the darkened areas onto the horizontal axes. The vertical lines at 0 and ± 169 km s^{-1} indicate the center of mass and the maximum Her X-1 velocities respectively. (c) A detail of the sum of all of the power spectra from the data. (d) The sum of all the power spectra in the 1.7-day orbital phase interval 0.5 - 0.7. The anomalous velocity feature is the peak just right of the 0 km s^{-1} marker.

Fig. 2. (a) The significant bins chosen from all of the power spectra are shown plotted as boxes on the orbital phase-frequency plane. Features I, II and III are labeled. The horizontal solid line and the solid sine curve indicate the average pulse frequency of Her X-1 and its doppler shifted pulse frequency respectively. The horizontal dashed lines at the top and bottom of the frame indicate the frequency region examined and are at twice the extent of the maximum Her X-1 doppler shift. The dotted lines indicate the regions on the phase-frequency plane which were applied to all of the spectra to calculate the amplitude profiles in (b) and (c). (b) The profile of amplitude vs orbital phase for Features I and II from HZ Her. (c) The amplitude profile following the doppler track of Her X-1. Feature III is indicated near phase 0.85. (d) The data coverage histogram over 24 equal parts of the 1.7-day orbital phase. The profiles in (b) and (c) have had this unevenness normalized out.

Fig. 3. The locations in the orbital plane (as projected for $i = 90^{\circ}$) of the strong pulsation events as derived from the precise measurements of f and f'. The boxes are fixed with respect to the centers of mass of Her X-1 and of the entire binary system. The positions of the center of mass of HZ Her and the dashed critical Roche lobe contour depend on the value of the mass ratio which was arbitrarily set equal to 1.7 (with HZ Her as the more massive component). The box lengths are set by the $\pm 1\sigma$ errors for the values of f'; the widths, by the $\pm 2\sigma$ errors for the f values. The arrows at the ends of the boxes indicate the direction of the Earth and (equivalently) the orbital phases at the midpoints of the runs. The scale is given at the lower right.

Fig. 4. (a) The precise frequencies for the 27 optical pulsation events of Features I, II and III are plotted vs Julian date. The Feature III frequencies are residuals from the doppler shifted Her X-1 track. (b) The individual mass ratios derived from the points of Features I and II are shown in (a) using Model 1 to match their individual velocities.

Fig. 5. The characteristic 35-day modulation of the optical pulsation amplitudes for (a) Feature I, (b) Feature II, and (c) Feature III. The vertical bars indicate the 67% confidence levels derived from the sum of one or more power spectrum bins near the frequency indicated by the insets at the upper right. The horizontal bars indicate the durations in orbital phase of the power spectra used for the plots. The horizontal axis indicates the 35-day phase in binary cycles. To show more clearly any variations on a short time scale, the restricted binary phase interval shown in the inset

has been expanded to fill each 35-day phase interval; thus the horizontal axis is discontinuous.

Fig. 6. The geometry for the reprocessing-reflection model calculations. HZ Her, Her X-1 and the x and y axes are shown to be rotating counter-clockwise (right-handedly) about the z axis.

Fig. 7. The pulsed amplitude vs 1.7-day orbital phase profiles for the three basic reprocessing-reflection models are shown above the data amplitude profile from Figure 2(b) for comparison.

Fig. 8. The Model 1 amplitude profiles vs 1.7-day orbital phase for three Roche equipotential contours with R = 1.65 are plotted together on the left for comparison. The right hand side shows the three contours associated with the profiles a, b, and c labeled according to their extent from the HZ Her c.m. toward Her X-1 along the mass axis. The critical Roche lobe defines 100% for this extent.

Fig. 9. (a) The Model 1 amplitude profile in orbital phase with R = 1.65 for the time-averaged reflection effect. The quantity $L_{opt}^{avg}/L_{X\text{-ray}}$ represents the ratio of flux from HZ Her to the flux from Her X-1 as seen from a direction near the orbital plane. (b) The Model 1 amplitude profile for the 1.24 s pulsed reflection effect. The flux from Her X-1 is assumed to be 100% pulsed. (c) The ratio of the profile in (b) to the profile in (a). This represents the degree of cancellation due to the time-of-flight integrations.

Fig. 10. The Model 1 frequency tracks over 1.7-day orbital phase for various mass ratios are plotted with the data events from Features I and II.

Fig. 11. The mass ratio of HZ Her - Her X-1 system derived from the data is plotted vs orbital inclination together with the R vs i curve obtained from the X-ray eclipse assuming HZ Her fills its Roche lobe. The region of intersection for the two results specifies the mass ratio and orbital inclination and thus determines the masses of HZ Her and Her X-1 (see text).

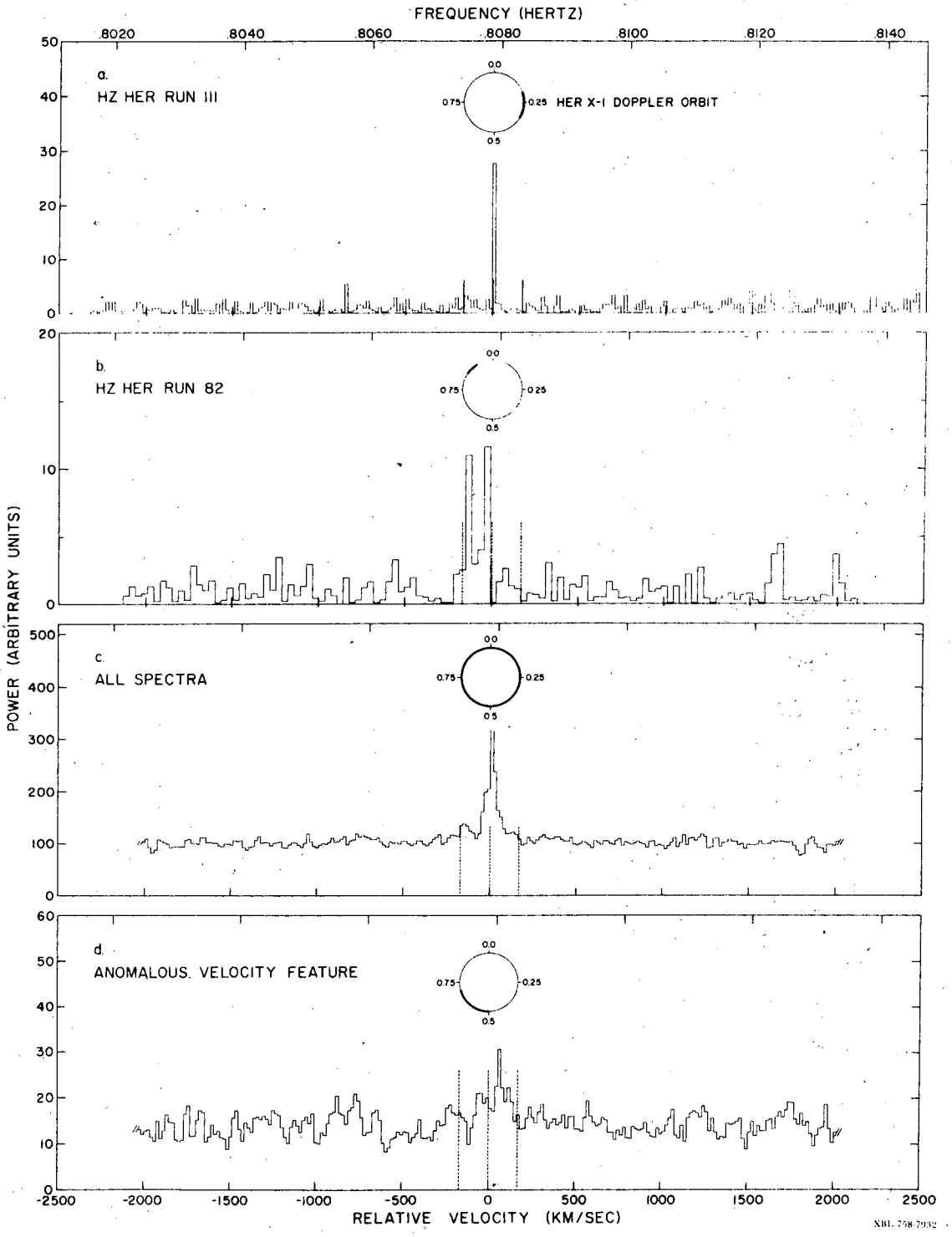

Fig. 1

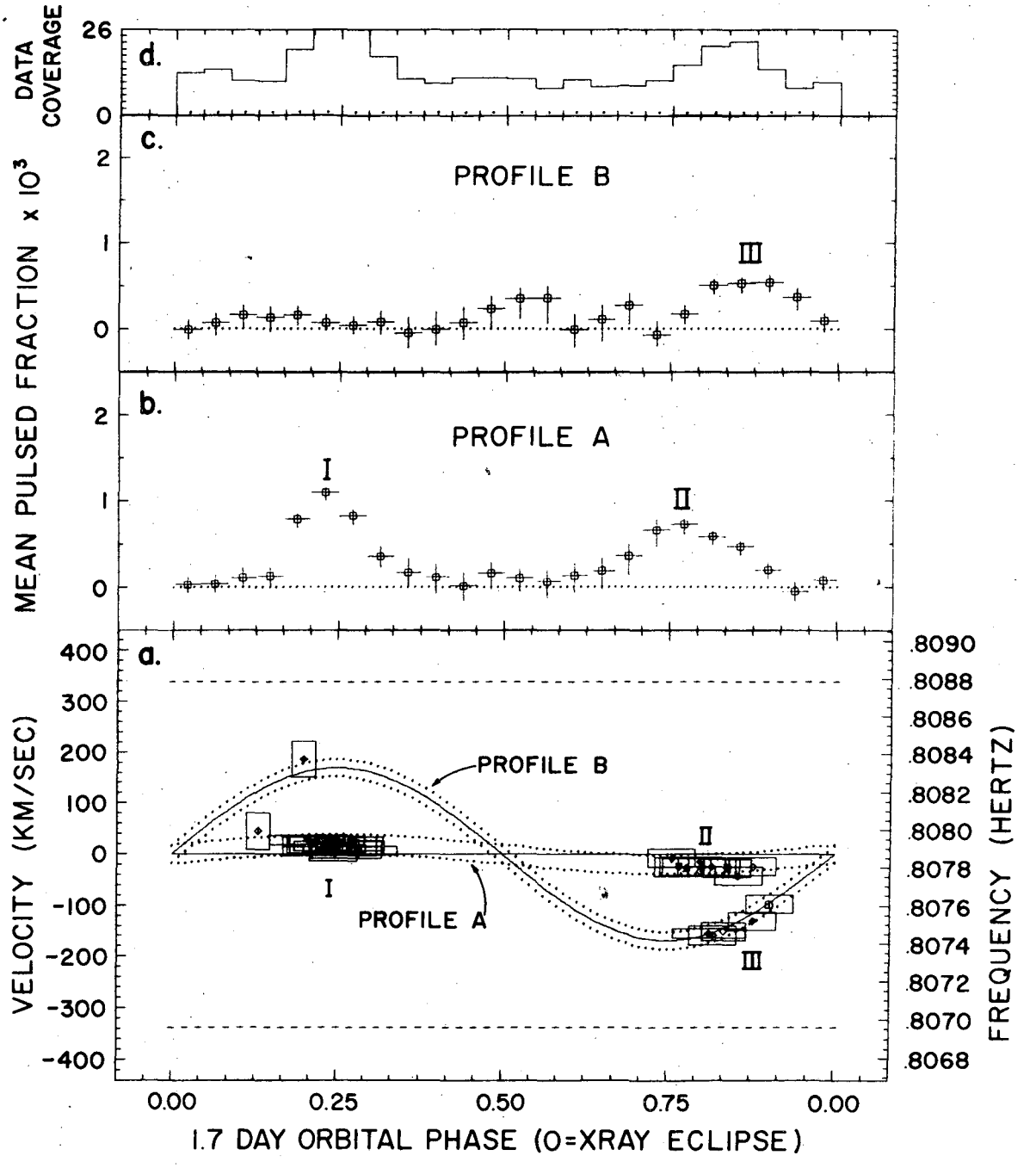

XBL 758-7931

Fig. 2

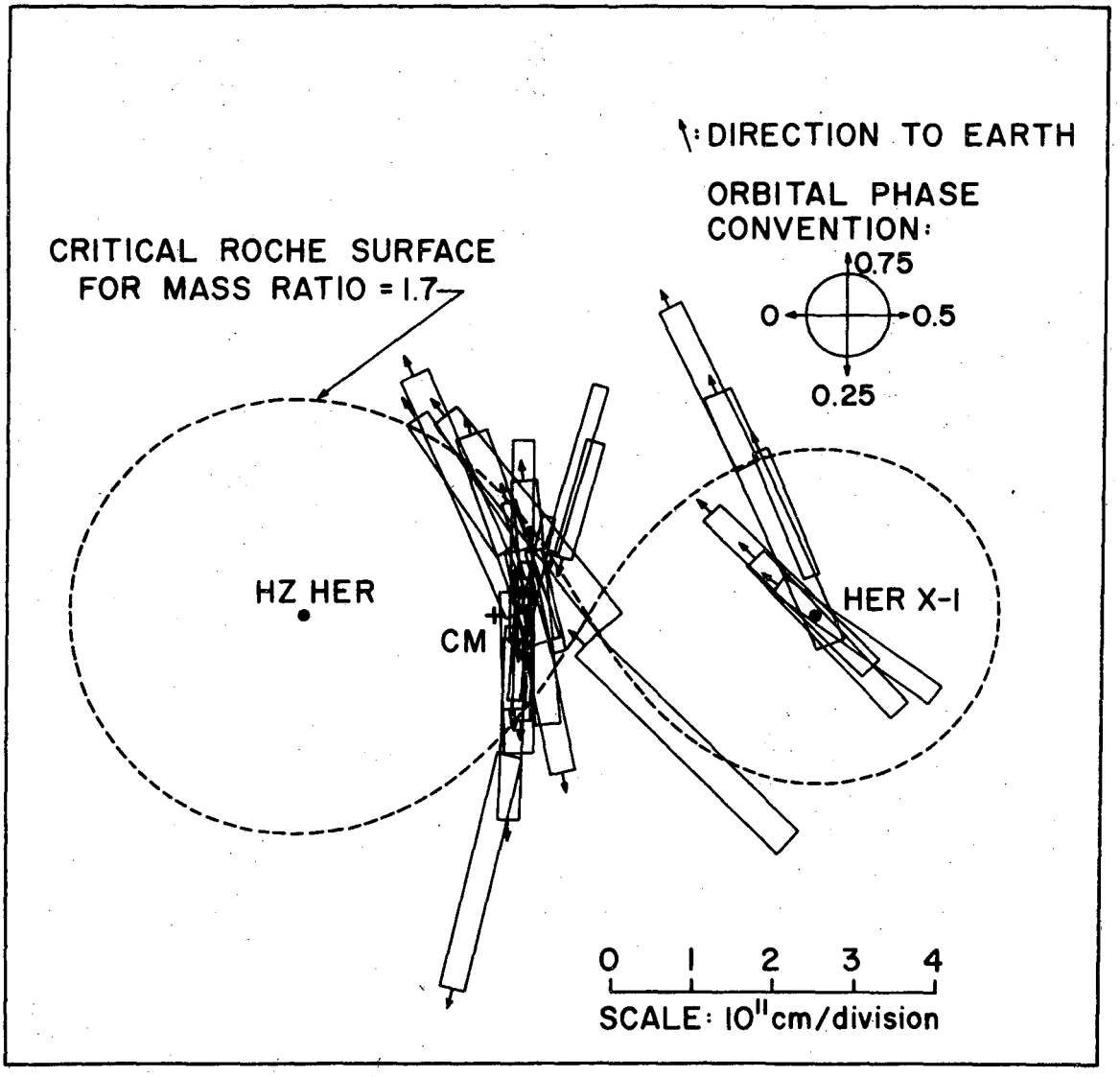

XBL 758-7930

Fig. 3

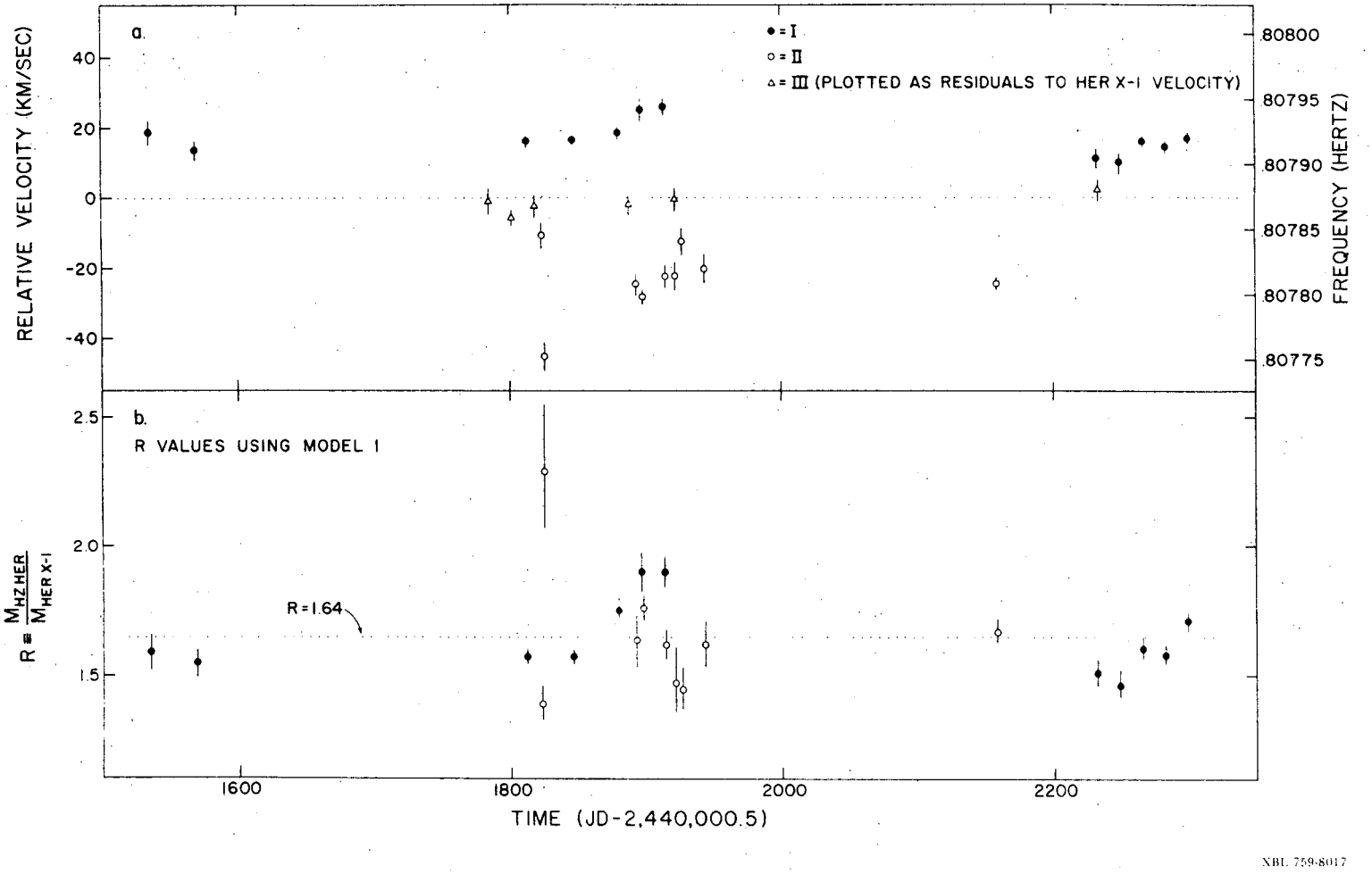
a.
●= I
○= II
△= III (PLOTTED AS RESIDUALS TO HER X-1 VELOCITY)
RELATIVE VELOCITY (KM/SEC)
FREQUENCY (HERTZ)
40
20
0
-20
-40
.80800
.80795
.80790
.80785
.80780
.80775
b.
R VALUES USING MODEL I
R = M_HZ HER / M_HER X-1
R=1.64
2.5
2.0
1.5
1600
1800
2000
2200
TIME (JD-2,440,000.5)
NBL 759-8017

Fig. 4

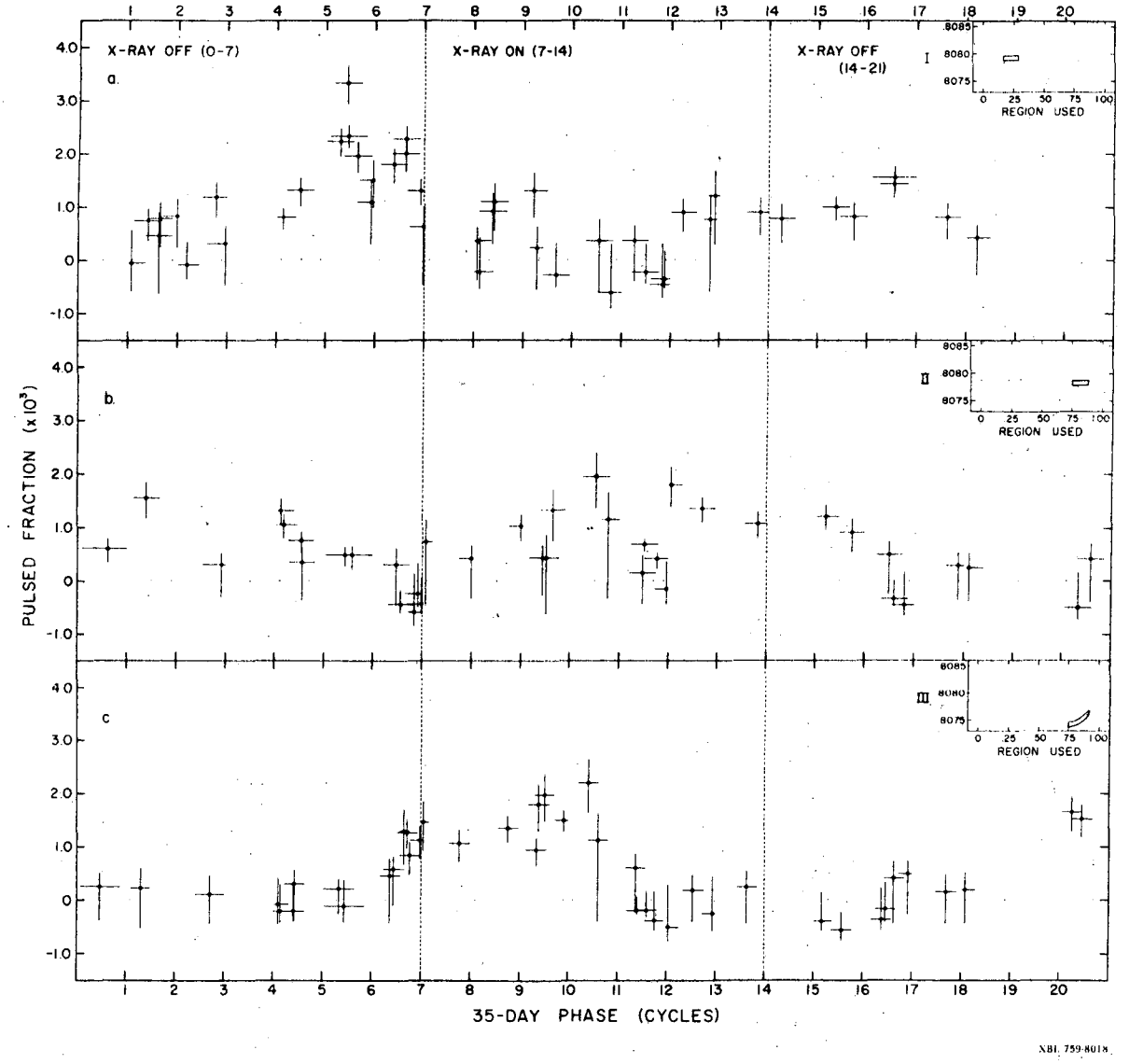
X-RAY OFF (0-7)
X-RAY ON (7-14)
X-RAY OFF (14-21)
a.
b.
c.
I
II
III
REGION USED
PULSED FRACTION (x10³)
35-DAY PHASE (CYCLES)
XBL 759-8018

Fig. 5

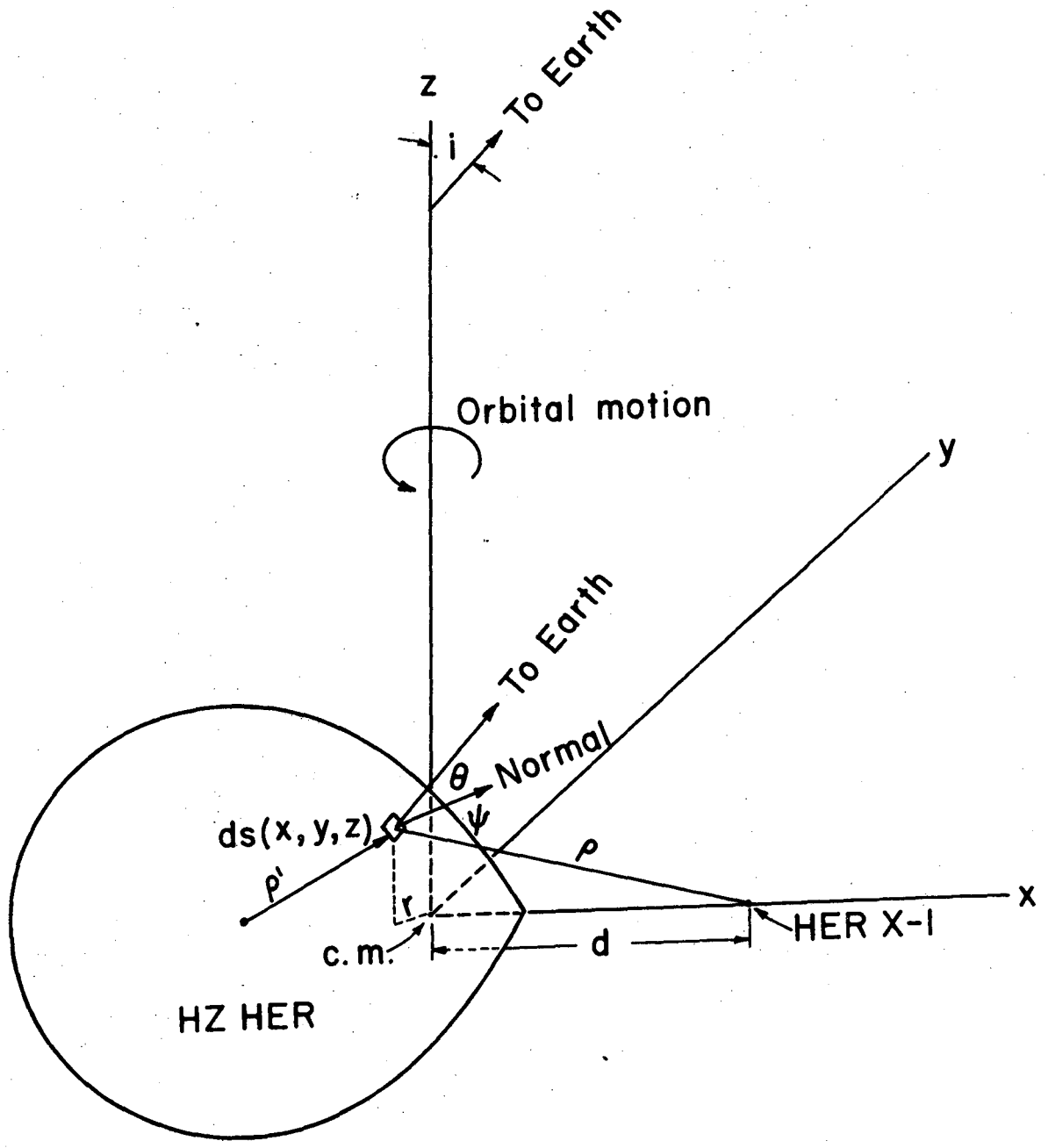

XBL 7510-8387

Fig. 6

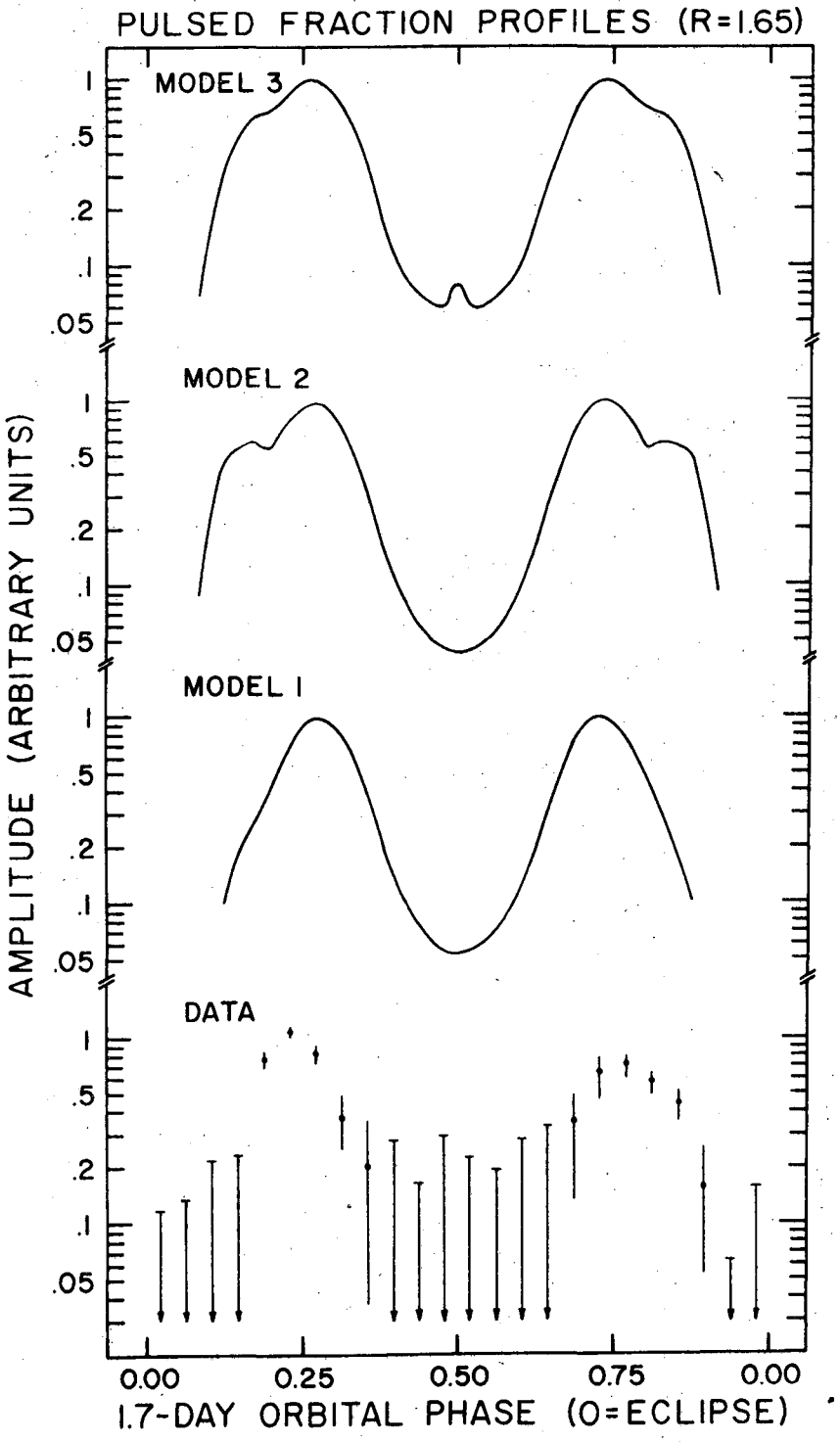

XBL 759-8205

Fig. 7

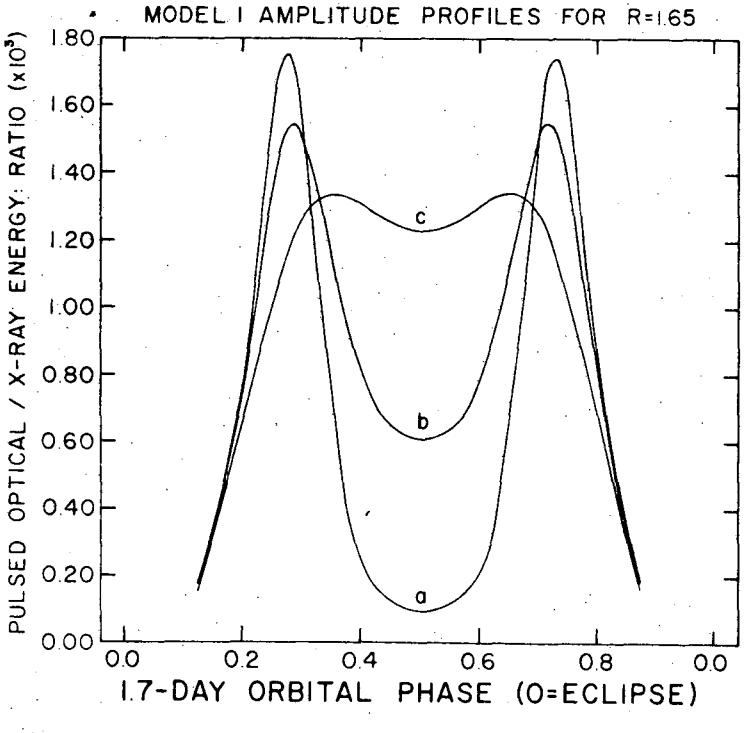

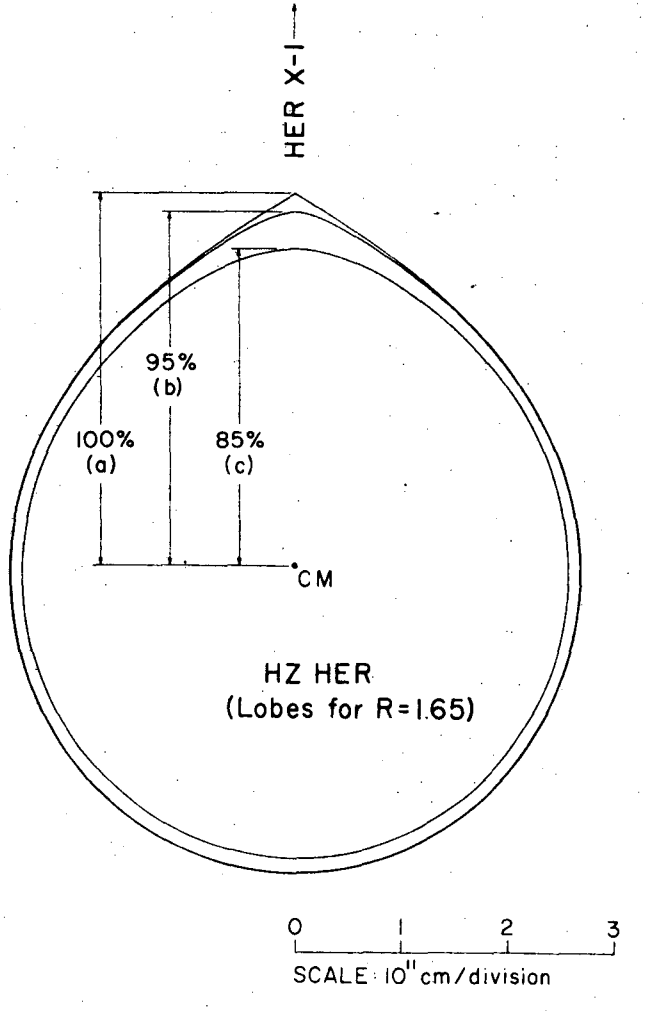

XBL 759-8141

Fig. 8

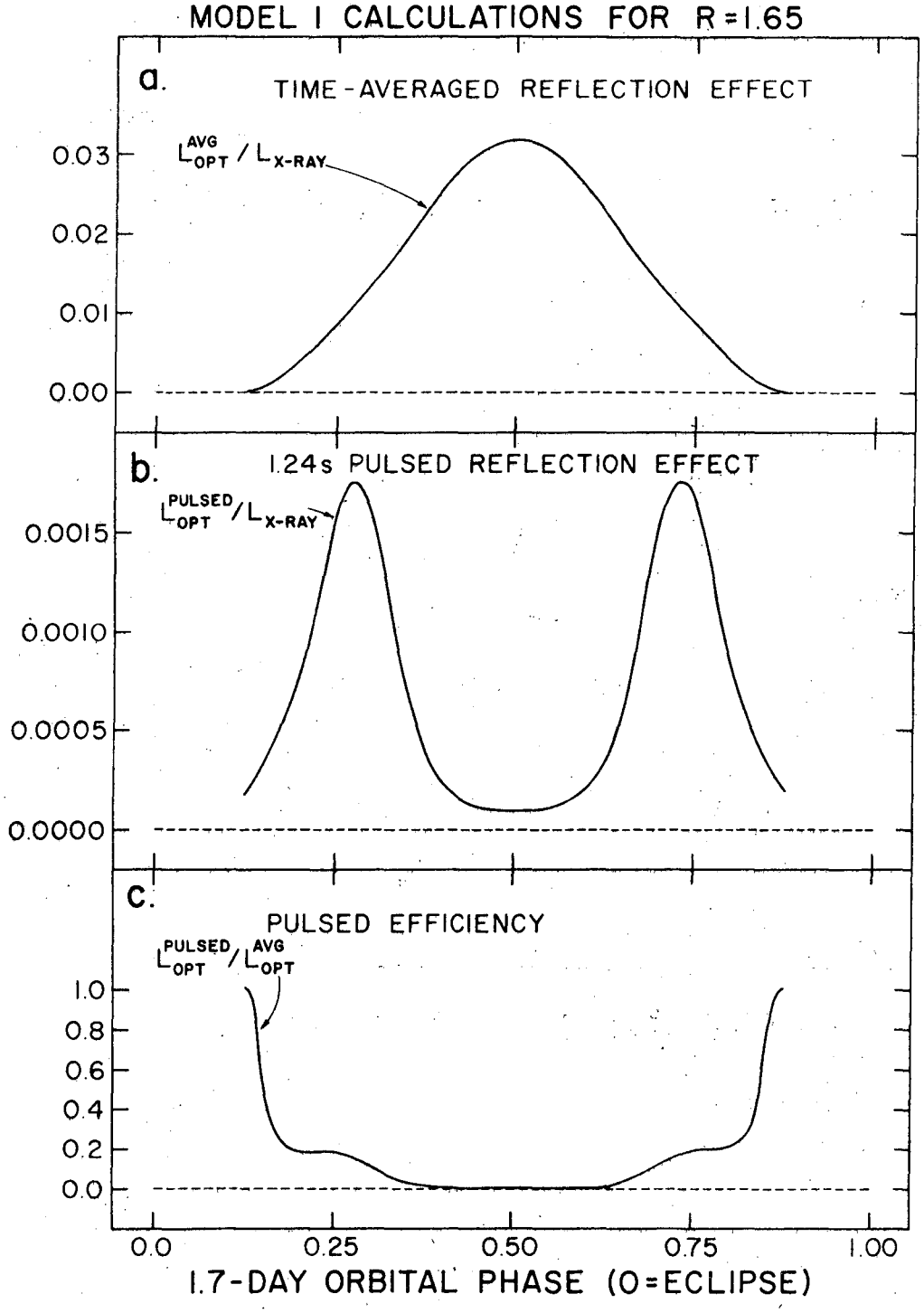

XBL 759-8099

Fig. 9

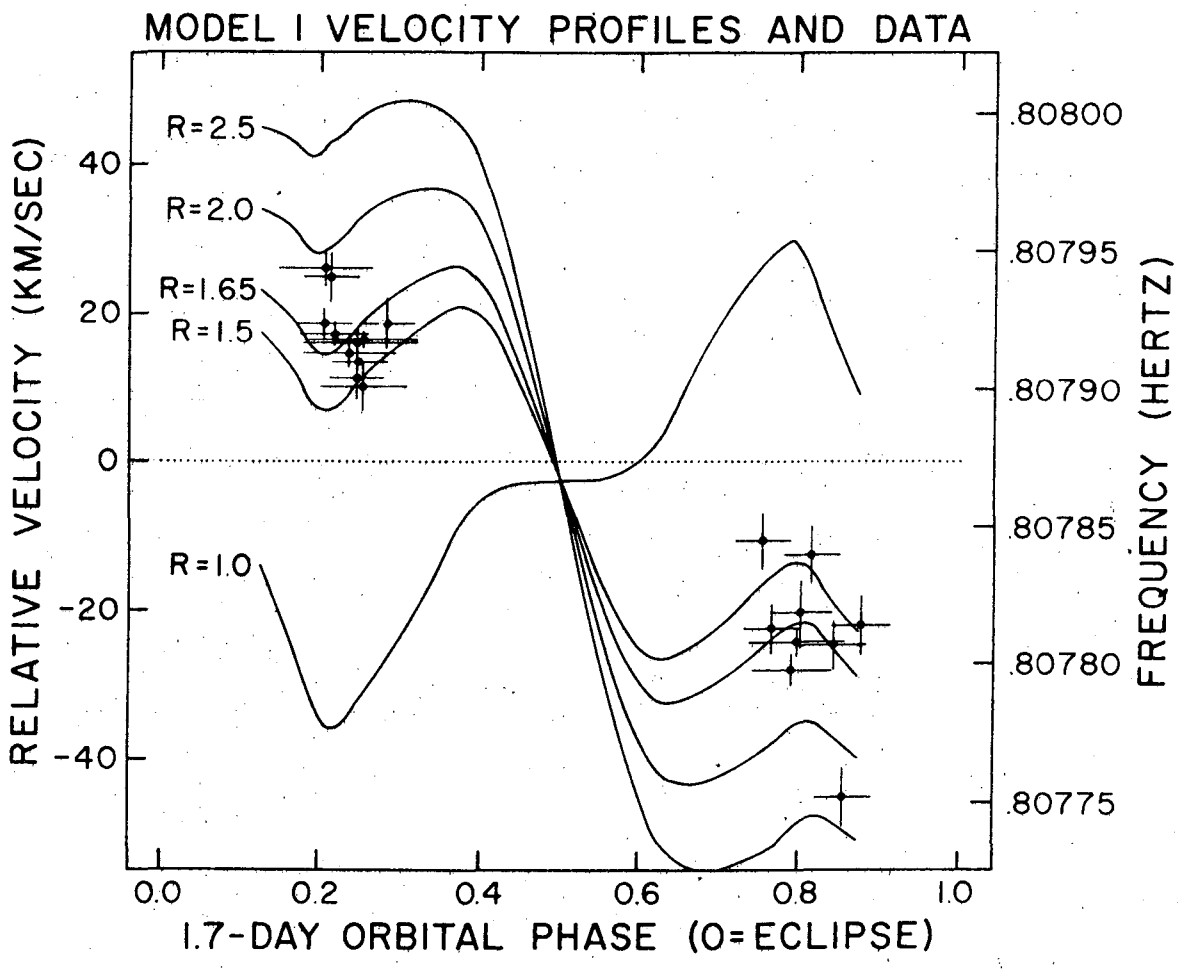

XBL 759-8097

Fig. 10

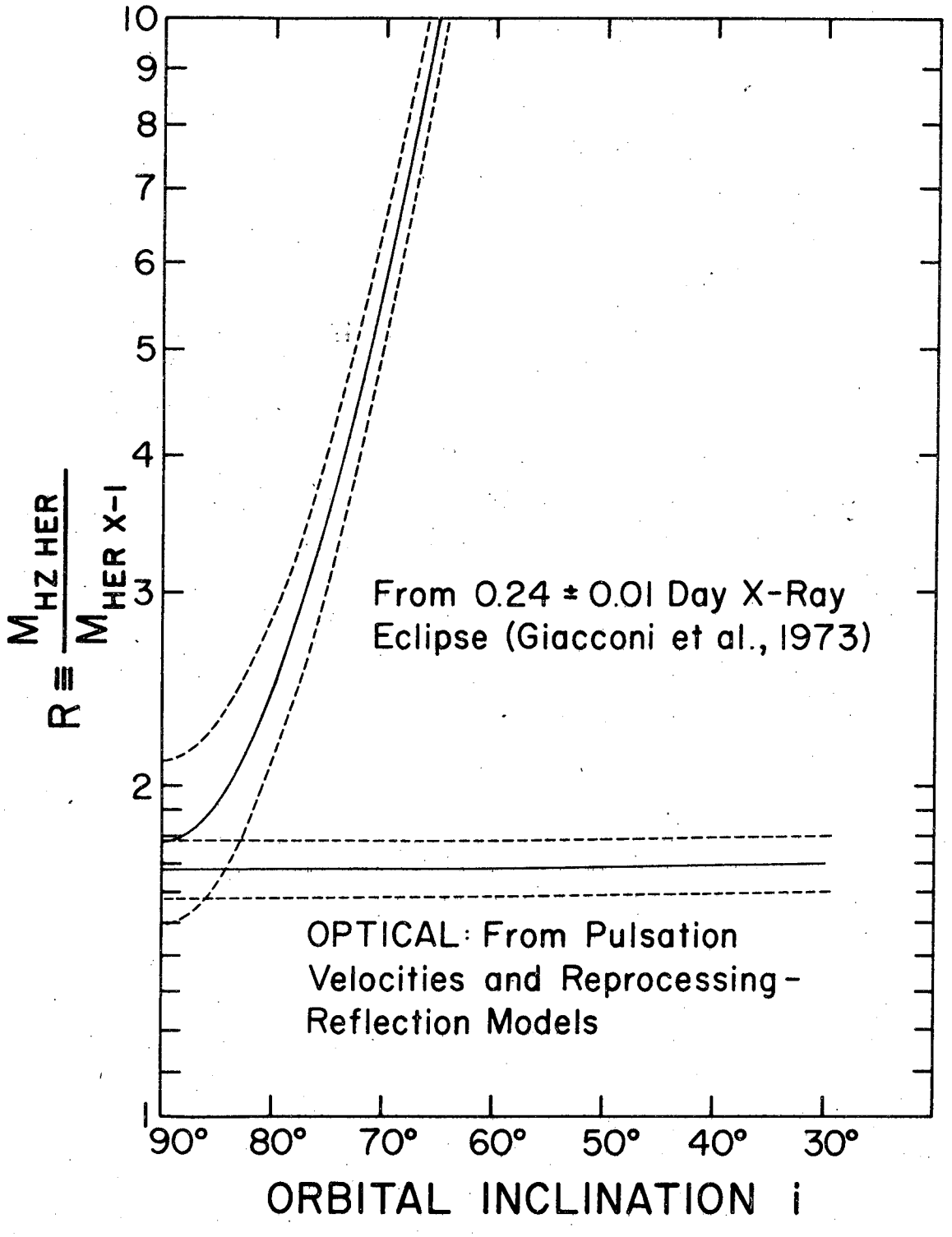

Fig. 11

TECHNICAL INFORMATION DIVISION
LAWRENCE BERKELEY LABORATORY
UNIVERSITY OF CALIFORNIA
BERKELEY, CALIFORNIA 94720